SUPPORTING INFORMATION APPENDIX

Table S1. Tight Entrance Cave mammal relative abundance data.

Table S2. Dose rates, paleodoses and optical ages for sediment samples from Tight Entrance and Kudjal Yolgah Caves

Table S3. $^{230}Th/^{234}U$ ages for samples of flowstone interbedded with fossil-bearing sediments in Tight Entrance Cave

Table S4. Summary of Tight Entrance Cave chronology

Table S5. Raw stable carbon- and oxygen-isotope data ($\delta^{13}C$, $\delta^{18}O$) from the shells of modern and fossil land snails (*Bothriembryon sayi*) utilized in this study

Table S6. Grand means of stable carbon- and oxygen-isotope data ($\delta^{13}C$, $\delta^{18}O$) from the shells of modern and fossil land snails (*Bothriembryon sayi*) utilized in this study

Table S7. $\delta^{13}C$ estimates of modern kangaroo diets in the Tight Entrance Cave region

Figure S1. Plan view of excavation area in the main chamber of Tight Entrance Cave

Figure S2. Near-complete skeleton of *'Procoptodon' browneorum* (WAM 08.1.600) from surface of Hatcher excavation area

Figure S3. Representative specimens from Tight Entrance Cave units B–F1

Figure S4. Representative specimens from Tight Entrance Cave units F2–J and reworked specimens from units H and J

Figure S5. Non-reworked specimens of extinct kangaroos from Kudjal Yolgah Cave

Figure S6. Examples of sectioning land snail samples from Tight Entrance Cave for stable isotope analysis.

Figure S7. Modeled land-snail $\delta^{18}O_{shell}$ versus $\delta^{18}O_{rain}$, for given temperature and relative humidity generated using the diffusive evaporation model of Balakrishnan and Yapp (2004)

Figure S8. Monthly averages of relative humidity and temperatures recorded at 9am at the Bureau of Meteorology weather station at Cape Leeuwin

Figure S9. Dietary $\delta^{13}C$ estimates for modern land snails and modern kangaroos, and modern and fossil land snails from Tight Entrance Cave

Figure S10. Interpreted stratigraphy of the southeast wall of the excavation

Figure S11. Untransformed linear regression of macrocharcoal against microcharcoal concentrations

PALEONTOLOGICAL EXCAVATIONS

The Tight Entrance Cave vertebrate fossil deposit was discovered by amateur paleontologist Lindsay Hatcher in 1991. A large pit was excavated by Hatcher and associates from 1992 to 1996 (denoted by a dashed line in Fig. S1), but without stratigraphic control. Fossils are now housed in the Vertebrate Palaeontology collection of the Department of Earth and Planetary Sciences, Western Australian Museum, Perth. They include the only specimens of the giant echidna *Megalibgwilia ramsayi*, extinct kangaroo *Sthenurus andersoni* and madtsoiid snake *Wonambi naracoortensis*, and the best-preserved specimens of the uncommon extinct kangaroo *'Simosthenurus' pales* thus far retrieved from the site. A near-complete skeleton of *'Procoptodon' browneorum* was collected from the sediment surface of the Hatcher excavation area, although the precise location was not recorded. Preservation is consistent with an origin from unit G or F2 (compare Figs. S2, S4), and the younger units H and J did not extend laterally into this area. Hatcher backfilled his excavation in late 1995 with the sediment extracted from the same pit and some *in situ* sediments from around the pit.

The Prideaux / Flinders University excavation commenced in January–February 1996. The excavation area was divided into a series of variably sized grids, with excavation proceeding according to unit using standard paleontological methods. Depths of unit boundaries were measured relative to a datum point established within an adjacent limestone slab. Excavated sediment was sieved and resultant residues of small vertebrate remains then dried and sorted (picked) for taxonomically identifiable remains. Larger bones were cleaned, dried and stabilized with polyvinyl butyrate dissolved in acetone. Specimens are reposited in the Department of Earth and Planetary Sciences, Western Australian Museum, Perth.

Stage 1 involved the excavation, in 10-cm horizontal levels, of a 1.5 x 1.0 m^2 pit. The main purpose was to facilitate a preliminary stratigraphic appraisal (Fig. S1). Stage 2 was excavated in July–August 1996 and involved connecting the stratigraphic pit with the Hatcher pit, which was simultaneously re-excavated and dry-sieved for vertebrate remains missed during the original mining operation. Following completion of the Stage 3 excavation (Fig. S1) the major sediment layers were designated units to which letters were ascribed from the unfossiliferous basal unit A to the uppermost unit J (Gully 1997). Subsequent excavation in 1999 (TEC-99) and 2007–2008 (TEC-A to TEC-O) revealed that units C and I were in fact spurious stratigraphic layers within Hatcher's backfill, which was more laterally extensive than Prideaux and Gully were originally made aware. While unit G is retained as a discrete unit, subsequent excavation revealed that it is largely a complex of moonmilk and flowstone formed on the surface of unit F2. Ages for unit G, F2, F1 and E are statistically indistinguishable (Ayliffe *et al.* 2008; Tables S2–S4).

Figure S1. Plan view of excavation area in the main chamber of Tight Entrance Cave. See above text for details on excavation stages and 1-m^2 quadrats. Spatial positions of optical dating samples (Table S2) are indicated by small bold numbers. Topographic heights (m) of sediment surface measured relative to datum. Grey shaded circles denote stalagmites.

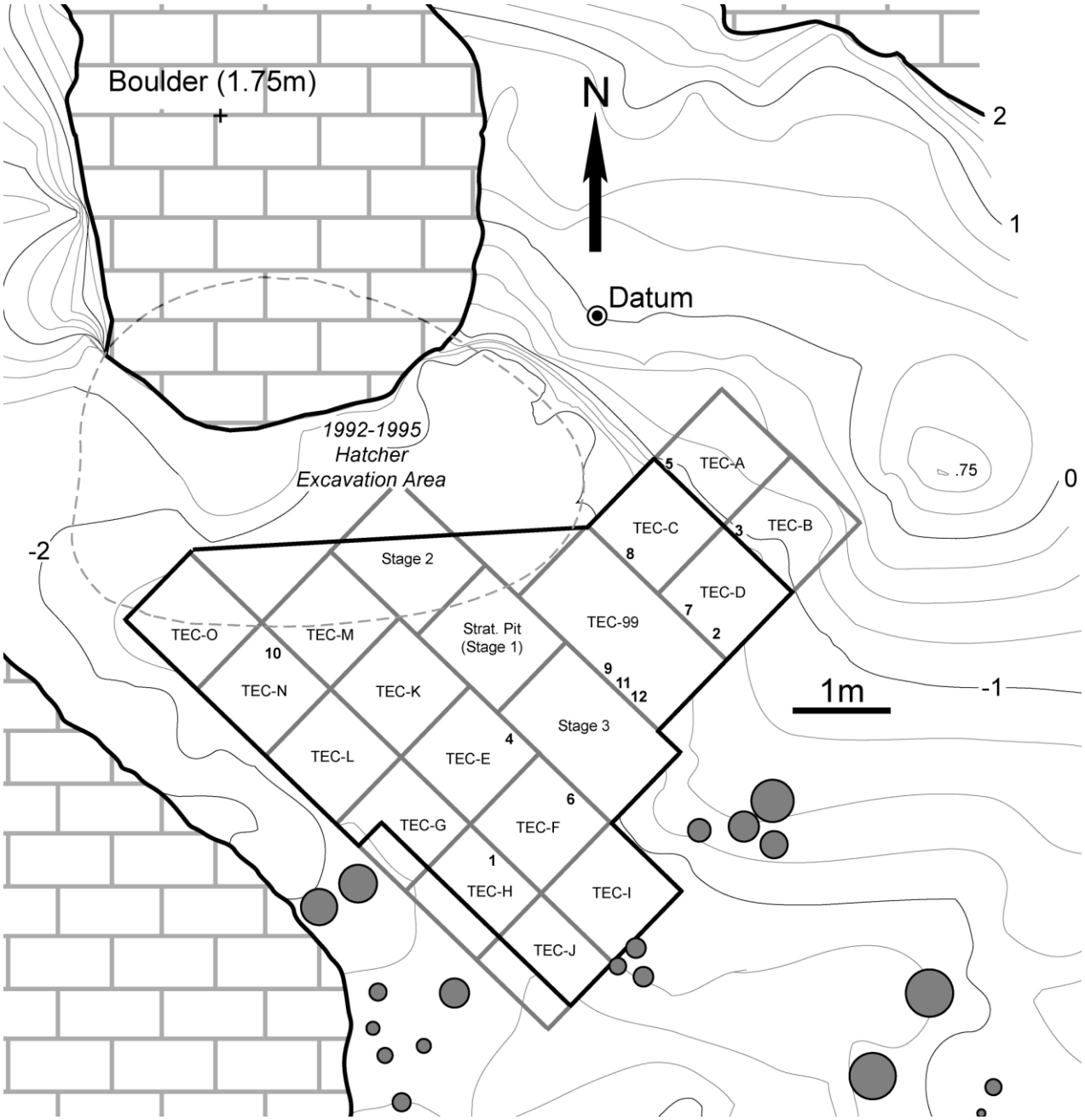

Figure S2. Near-complete skeleton of *'Procoptodon' browneorum* (WAM 08.1.600) from the surface of the Hatcher excavation area, Tight Entrance Cave. Preservation matches material excavated from units G and F2 in the Prideaux excavation.

FAUNAL DATA

Table S1. Tight Entrance Cave mammal relative abundance data. NISP, number of identified specimens; MNI, minimum number of individuals.

Species[1]	Body Mass[2] (kg)	Relative Abundance ($MNI_{species}/MNI_{total}$ %)					
		Unit B	Unit D	Unit E*	Units E–G	Unit H	Unit J
Tachyglossus aculeatus	4.5	0.0	0.3	0.0	0.0	0.0	0.0
Megalibgwilia ramsayi	10	0.0	0.3	0.0	0.0	0.0	0.0
Thylacinus cynocephalus	25	1.1	1.7	2.0	2.8	2.4	1.2
Dasyurus geoffroii	1.1	8.7	9.3	8.0	11.3	4.9	7.1
Dasycercus cristicauda	0.13	0.0	0.3	0.0	0.0	0.0	0.0
Sarcophilus harrisii	9.0	2.2	0.7	2.0	1.4	4.9	1.2
Antechinus flavipes	0.04	1.1	0.7	0.0	2.8	0.0	0.0
Isoodon obesulus	0.78	1.1	1.0	0.0	1.4	2.4	0.0
Perameles bougainville	0.23	1.1	4.0	2.0	1.4	0.0	11.8
Phascolarctos cinereus	8.0	1.1	1.0	2.0	0.0	0.0	0.0
Vombatus hacketti	26	1.1	1.3	2.0	2.8	0.0	0.0
Vombatidae sp. indet.	300	0.0	0.0	2.0	0.0	0.0	0.0
Zygomaturus trilobus	500	1.1	1.0	4.0	1.4	0.0	0.0
Thylacoleo carnifex	104	1.1	0.7	2.0	1.4	0.0	0.0
Pseudocheirus occidentalis	1.0	0.0	2.0	0.0	5.6	14.6	5.9
Trichosurus vulpecula	4.0	1.1	1.0	2.0	2.8	7.3	23.5
Bettongia lesueur	0.68	0.0	0.3	0.0	1.4	4.9	3.5
Bettongia penicillata	1.3	2.2	0.7	4.0	0.0	0.0	4.7
Borungaboodie hatcheri	10	0.0	0.3	0.0	0.0	0.0	0.0
Potorous gilbertii	0.95	2.2	1.7	4.0	7.0	14.6	3.5
Congruus kitcheneri	40	0.0	0.7	0.0	0.0	0.0	0.0
Macropus fuliginosus	49	10.9	9.0	4.0	4.2	4.9	5.9
Macropus eugenii	2.1	0.0	0.3	0.0	0.0	0.0	0.0
Macropus irma	8.0	7.6	3.0	4.0	4.2	4.9	7.1
Macropus sp. nov.	23	1.1	1.3	2.0	0.0	0.0	0.0
Petrogale lateralis	4.0	0.0	0.0	0.0	1.4	0.0	8.2
Protemnodon sp. cf. *P. roechus*	166	1.1	0.7	4.0	1.4	0.0	0.0
Setonix brachyurus	3.0	29.3	30.0	32.0	28.2	14.6	10.6
Sthenurus andersoni	72	0.0	0.3	0.0	0.0	0.0	0.0
Metasthenurus newtonae	55	1.1	0.3	0.0	0.0	0.0	0.0
'Procoptodon' browneorum	60	17.4	15.0	6.0	8.5	4.9[3]	0.0
Simosthenurus occidentalis	118	4.3	5.0	4.0	5.6	2.4[3]	0.0
'Simosthenurus' pales	150	1.1	1.3	4.0	1.4	0.0	0.0
Notomys sp. indet.	0.05	0.0	0.0	0.0	0.0	2.4	1.2
Pseudomys albocinereus	0.03	0.0	0.0	0.0	0.0	0.0	1.2
Pseudomys occidentalis	0.03	1.1	0.7	2.0	0.0	0.0	0.0
Pseudomys shortridgei	0.07	0.0	0.7	0.0	0.0	0.0	0.0
Rattus fuscipes	0.14	0.0	3.3	2.0	1.4	9.8	3.5
No. species >5kg		14	18	14	11	6	4
No. species <5kg		9	16	8	11	9	12
Total MNI		92	300	50	71	41	85
Total NISP		213	712	148	123	88	201

[1] *Phascogale calura* and *Sminthopsis crassicaudata* were collected from disturbed sediments; their precise stratigraphic provenance is unknown.

[2] Mean body masses derived from van Dyck & Strahan (2008) for extant species and Wroe *et al.* (2004), Johnson & Prideaux 2004 and Helgen *et al.* (2006) for extinct species.

[3] Reworked from older strata (Fig. S4).

Paleoecology

Numbers of identifiable specimens for each species were recorded in spreadsheets according to grid, level and unit. From this the minimum numbers of individuals (MNI) for each species within stratigraphic units was calculated (Table S1). MNI is an estimate of the lowest number of animals that would account for all identified specimens of a species. Here, it is a measure of the most abundant of four elements: left or right maxillary specimen, or left or right dentary specimen. Relative abundance (MNIspecies/MNItotal%) is the most widely utilized measure of species incidence.

Variations in fossil samples sizes for different stratigraphic levels or sites greatly influence determinations of species richness (Raup 1974; Barnosky *et al.* 2004, 2005). Rarefaction analysis using Analytic Rarefaction version 1.3 developed by Steven M. Holland (http://www.uga.edu/strata/software/) was undertaken to examine the influence of sample size differences in species richness values obtained for small mammals in the Tight Entrance Cave units (large mammal samples sizes are too low for rarefaction analysis to be useful). Since the lowest NISP was recorded for Units E* and H (NISP = 69), we used this value for all units to produce a standardized plot of expected species richness for small mammals through the sequence (Fig. 4A).

Reworking of large mammal specimens in units H and J

Fossils from each stratigraphic unit within the Tight Entrance Cave deposit are distinctly preserved, particularly with regard to bone texture, degree of mineralization, surface etching, bone color and sedimentary patina texture and color (Figs. S3, S4). As a consequence it is possible to determine the stratigraphic origin of most bones retrieved from the deposit simply from their external features. This is very helpful for assessing the likelihood of reworking of fossils from older underlying units into younger, higher units. Of particular interest are fragmentary specimens of two large sthenurine kangaroo species, *Simosthenurus occidentalis* and *'Procoptodon' browneorum*, collected from units H and J, dated at between 34 and 30 ka (Table S1; main text). These include individual teeth or tooth fragments, which are light yet hardy and commonly reworked in cave contexts, but also cranial and limb fragments. All are consistent with an origin from within units B, D, E* or F1 as judged from bone and patina characteristics (Figs. S3, S4). Bones sampled contained insufficient collagen for direct ^{14}C dating (Oxford Radiocarbon Accelerator Unit, pers. comm., 24 April 2009).

The youngest reliable date on extinct Pleistocene kangaroos from southwestern Australia is an OSL age of 40 ± 2 ka on sand grains collected immediately adjacent to articulated specimens of *'Procoptodon' browneorum* and *Protemnodon roechus* from Kudjal Yolgah Cave (Fig. S5), 5 km south of Tight Entrance Cave (Fig. 1).

Figure S3. Representative specimens from Tight Entrance Cave Units B, D, E* and F1.

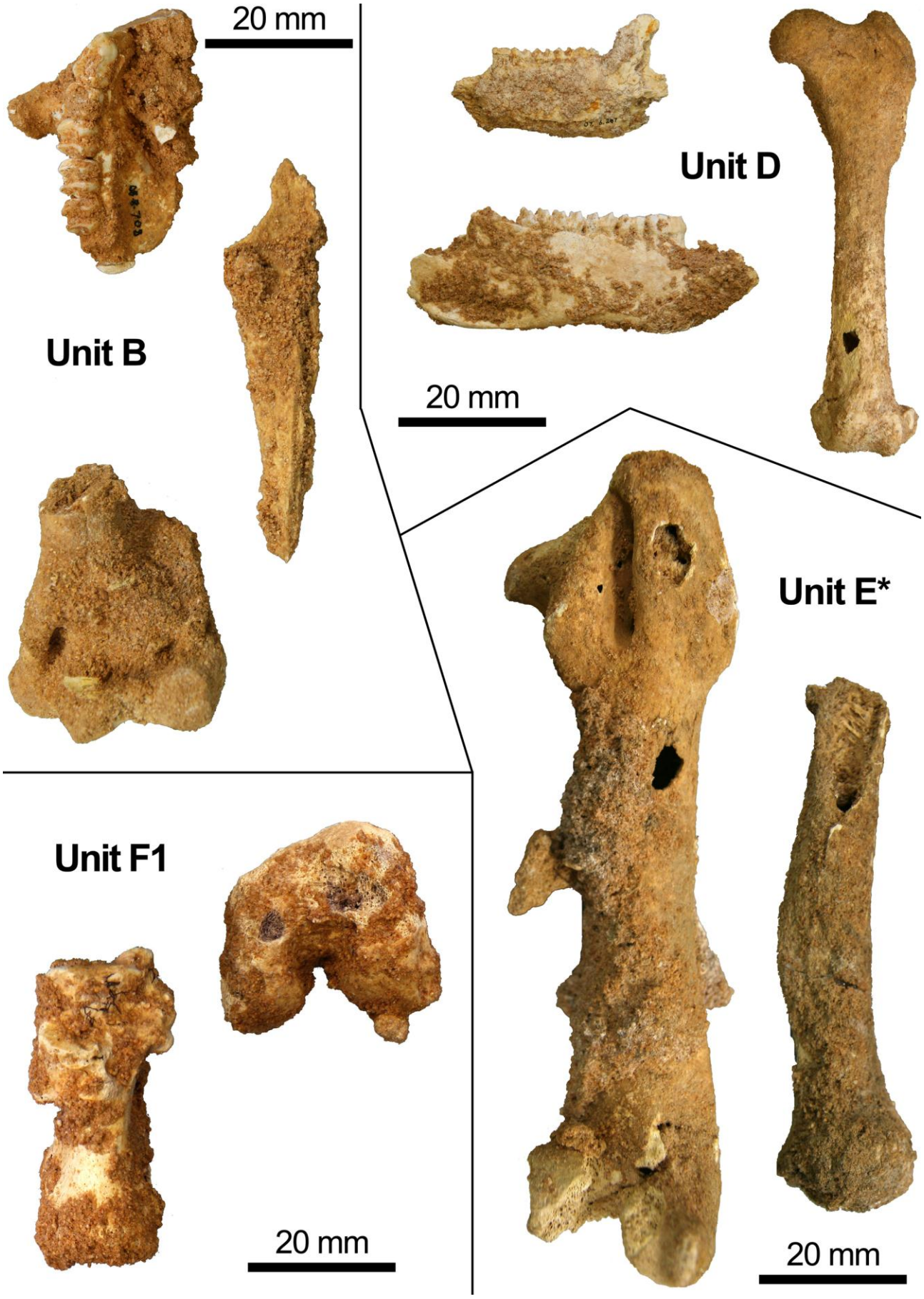

Figure S4. Representative specimens from Units F2 through J and fragmented specimens from units H and J with preservations matching an origin within units B, D, E* and/or F1.

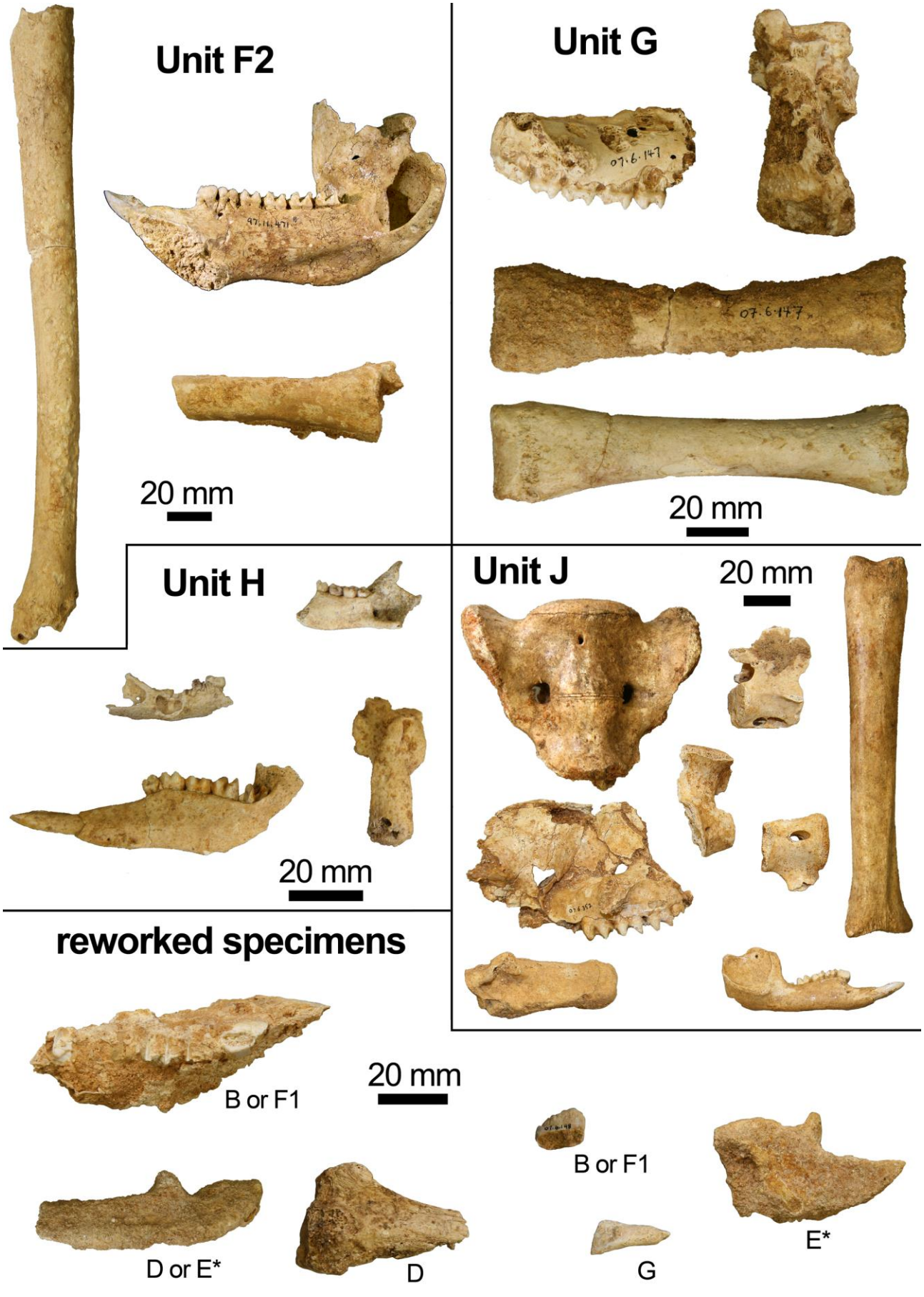

Figure S5. Non-reworked specimens of extinct kangaroos from Kudjal Yolgah Cave. Dated to 40 ± 2 ka (KYC3), these represent the youngest-known articulated or associated remains from mainland Australia of species that failed to survive the Pleistocene. **a**, Associated left and right forelimb elements of *Protemnodon* sp. cf. *roechus* (P.r.). **b**, Articulated hind foot (1) and three caudal vertebrae (2) of *'Procoptodon' browneorum* (P.b.). **c**, Southside of excavation showing location of partly excavated P.r. and unexcavated P.b. specimens relative to KYC3 sample hole. The flowstone capping the Pleistocene cone has produced U-Th ages of 33.6 ± 0.8 to 35.4 ± 0.5 ka (Roberts *et al.* 2001).

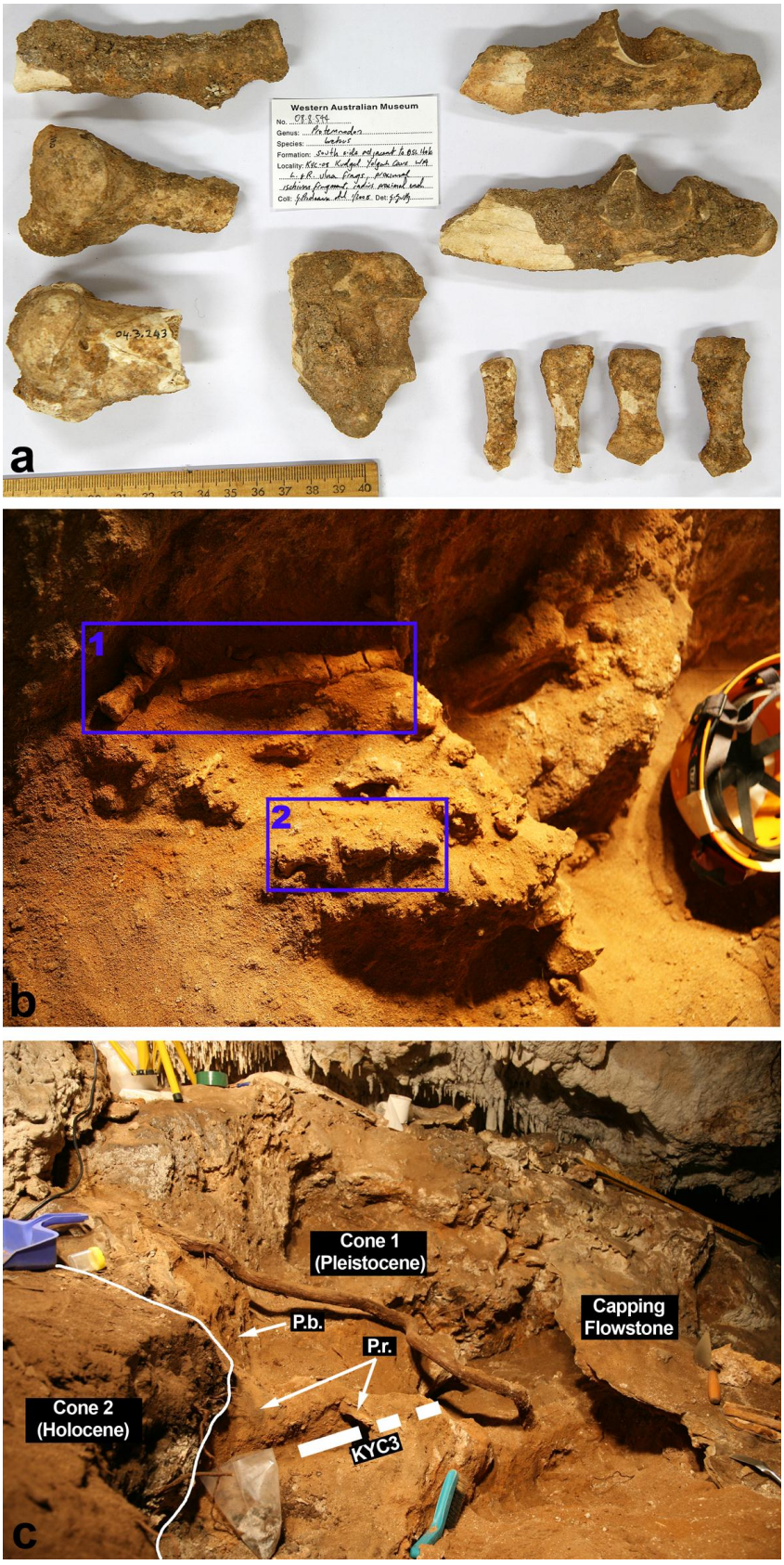

CHRONOLOGY

Optical Dating

Optical dating provides an estimate of the time elapsed since luminescent mineral grains, such as quartz and feldspar, were last exposed to sunlight (Huntley *et al*. 1985; Aitken 1998). The event being dated in this study is the time of entry of sediment grains into Tight Entrance Cave. Once buried, grains are exposed to an ionizing radiation flux (the 'dose rate') from the decay of radioactive elements in the surrounding deposit, with minor contributions from cosmic rays and from radioactive inclusions inside the grains. The absorbed radiation energy results in the steady accumulation of a trapped charge, and the corresponding radiation dose (the 'paleodose') can be estimated using the optically stimulated luminescence (OSL) signal. The optical age is then calculated by dividing the paleodose by the dose rate.

We collected samples under light-safe conditions and extracted quartz grains of 180–212 μm in diameter in the laboratory under dim red illumination using standard procedures; this included an etch with 48% hydrofluoric acid for 40 min to remove the alpha-irradiated rind of each grain (Aitken 1998). Paleodoses were determined for individual quartz grains using the single-aliquot regenerative-dose (SAR) protocol, instrumentation, and methods of data collection and analysis described elsewhere (Murray & Roberts 1998; Galbraith *et al*. 1999; Murray & Wintle 2000).

OSL measurements were made on individual grains, rather than on multi-grain aliquots, in order to (1) check the stratigraphic integrity of the deposit, (2) assess if the grains had been exposed originally to sufficient sunlight to empty the OSL traps, and (3) reject grains with aberrant physical properties from the sample, and thereby obtain more accurate and precise optical ages (Jacobs *et al*. 2006; Jacobs & Roberts 2007).

Optical stimulation of individual grains was achieved using green (532 nm) light from a 10 mW Nd:YVO_4 solid-state diode-pumped laser, with the beam focused onto a spot of ~10 μm in diameter. For each grain, the OSL signals induced by the natural and regenerative doses were measured for 2 s at an elevated temperature of 125°C, following a preheat of 240°C for 10 s. A preheat of 160°C for 5 s was applied to the test doses, which are used to correct for any sensitivity changes between SAR measurement cycles. The ultraviolet OSL emissions were detected using an EMI 9635Q photomultiplier tube fitted with Hoya U340 filters, and laboratory doses were given using a calibrated $^{90}Sr/^{90}Y$ beta source. The paleodose for each grain was calculated from the first 0.2 s of OSL decay, with the mean count rate over the final 0.3 s of stimulation subtracted as background.

Standard tests of SAR protocol performance were made, including dose recovery tests, checks on the extent of thermal transfer, and use of a replicate regenerative dose during the measurement

sequence to assess the adequacy of the test-dose sensitivity correction (Galbraith *et al*. 1999; Murray & Wintle 2000; Jacobs *et al*. 2006). We found no significant problems.

Of the 12 samples measured from Tight Entrance Cave, two (TEC99–unit A and TEC07–1) were considered to consist of populations of well-bleached grains, based on the extent of paleodose 'overdispersion' (i.e., the scatter among the paleodose estimates after taking into account all measurement uncertainties) and on the distribution pattern of the paleodoses when displayed as radial plots. For both of these samples, as well as sample KY3 from Kudjal Yolgah Cave, the weighted mean paleodose was determined using the central age model (Galbraith *et al*. 1999). The remaining 10 samples were thought to consist of multiple populations of well-bleached grains, with younger grains having been mixed in the darkness of the cave with older grains derived from pre-existing deposits en route to the main fossil chamber. For these samples, the paleodose associated with the population of grains bleached most recently was estimated using the minimum age model (Galbraith *et al*. 1999).

The total dose rate for each sample was calculated as the sum of the beta and gamma dose rates due to the radioactive decay of ^{238}U, ^{235}U, ^{232}Th (and their daughter products) and ^{40}K, plus the internal and cosmic-ray dose rates. The beta dose rates were deduced from high-resolution gamma spectrometry measurements (for samples with prefix TEC07) or from beta counting using a Risø GM-25-5 beta counter, making allowances for beta-dose attenuation. An *in situ* gamma dose rate was measured for all samples, except for TEC–E, TEC07–4 and TEC07–1. For the latter pair, the gamma dose rate was determined from high-resolution gamma spectrometry measurements, whereas a combination of thick-source alpha counting and beta counting was employed for sample TEC–E. For all samples, the beta and gamma dose rates were calculated for a water content of 5 ± 2%. Account was also taken of the cosmic-ray contribution (adjusted for site altitude, geomagnetic latitude, and thickness of rock and sediment overburden; Prescott & Hutton 1994) and the effective internal alpha dose rate (estimated from measurements made on quartz from southeastern Australia; Bowler *et al*. 2003).

Table S2 provides the paleodose and dose rate information for each of the Tight Entrance Cave samples (and for KY3), together with their optical ages, which are in correct stratigraphic order.

Table S2. Dose rates, paleodoses and optical ages for sediment samples from Tight Entrance and Kudjal Yolgah Caves. See Fig. S1 for sample spatial positions.

Sample Spatial Position No.	Sample name	Unit	Field water content (%)[1]	Dose rate (Gy ka^{-1})			Total dose rate (Gy ka^{-1})[5]	Paleodose (Gy)[6]	Age model used[7]	No. of grains	σ_d (%)[8]	OSL age (ka)[9]
				Beta[2]	Gamma[3]	Cosmic[4]						
1	TEC–H	H	5 ± 2	0.28 ± 0.01	0.32 ± 0.01	0.023 ± 0.002	0.65 ± 0.03	21 ± 2	MAM	194	57 ± 3	32 ± 3
2	TEC07–5	H	5 ± 2	0.27 ± 0.01	0.24 ± 0.01	0.023 ± 0.002	0.56 ± 0.02	19 ± 1	MAM	416	38 ± 2	34 ± 2
3	TEC07–4	F2	5 ± 2	0.31 ± 0.01	0.40 ± 0.01	0.023 ± 0.002	0.77 ± 0.04	36 ± 2	MAM	353	41 ± 2	47 ± 3
4	TEC–E	F1	5 ± 2	0.32 ± 0.04	0.43 ± 0.02	0.023 ± 0.002	0.80 ± 0.06	36 ± 2	MAM	251	33 ± 2	45 ± 4
5	TEC07–3	F1	5 ± 2	0.29 ± 0.02	0.30 ± 0.01	0.023 ± 0.002	0.64 ± 0.03	34 ± 4	MAM	336	39 ± 2	53 ± 4
6	TEC–F	E*	5 ± 2	0.35 ± 0.01	0.36 ± 0.01	0.023 ± 0.002	0.76 ± 0.03	53 ± 2	MAM	227	32 ± 2	70 ± 4
7	TEC07–6	D	5 ± 2	0.27 ± 0.01	0.33 ± 0.01	0.023 ± 0.002	0.66 ± 0.02	59 ± 3	MAM	304	36 ± 2	89 ± 6
8	TEC–C	D	5 ± 2	0.38 ± 0.01	0.27 ± 0.01	0.023 ± 0.002	0.71 ± 0.03	67 ± 4	MAM	197	31 ± 3	95 ± 7
9	TEC99–unit D	D	5 ± 2	0.30 ± 0.01	0.31 ± 0.01	0.023 ± 0.002	0.66 ± 0.03	64 ± 4	MAM	144	33 ± 3	98 ± 8
10	TEC–N	D	5 ± 2	0.34 ± 0.01	0.30 ± 0.01	0.023 ± 0.002	0.69 ± 0.03	71 ± 3	MAM	200	22 ± 2	103 ± 7
11	TEC07–1	B	5 ± 2	0.42 ± 0.02	0.52 ± 0.01	0.023 ± 0.002	0.99 ± 0.04	133 ± 4	CAM	184	26 ± 3	135 ± 7
12	TEC99–unit A	A	5 ± 2	0.36 ± 0.02	0.23 ± 0.01	0.023 ± 0.002	0.64 ± 0.03	146 ± 4	CAM	172	24 ± 2	227 ± 13
-	KY3[10]	6	5 ± 2	0.54 ± 0.03	0.40 ± 0.01	0.13 ± 0.01	1.11 ± 0.05	44 ± 1	CAM	205	25 ± 2	40 ± 2

1. In situ gamma spectrometry components were measured at respective field water contents (0.1–1.4 %), whereas beta counting, thick-source alpha counting and high-resolution gamma spectrometry measurements were made on dried sediment samples. All dose rate components were then readjusted to a value of 5 ± 2 %. This value was chosen as it encompasses the range of present water contents and is likely to reflect past water contents at the site. Field water content was calculated as the mass of water expressed as a percentage of the mass of dry sample.

2. Mean ± standard (1σ) error, determined by beta counting for all samples, except TEC07 samples which were determined by high-resolution gamma-spectrometry.
3. In situ gamma dose rates for all samples, except TEC–E, TEC07–4 and TEC07–1, were measured at field water content before being adjusted to a value of 5 ± 2 %. Gamma dose rates for TEC07–4 and TEC07–1 were determined using high-resolution gamma-spectrometry, while the gamma dose rate for TEC–E was calculated using a combination of thick-source alpha counting and beta counting. Relative standard errors for the in situ measurements are estimated at 2.5%.
4. Estimated using published relationships (Prescott & Hutton 1994) using a latitude of 34° south, a longitude of 155° east, an altitude of 50 m, sediment and rock densities of 2.0 g cm^{-3} and 1.2 g cm^{-3}, respectively, and a constant rock overburden of 15 m.
5. Mean ± total (1σ) uncertainty, calculated as the quadratic sum of the random and systematic uncertainties. Total dose rate includes a 0.03 Gy ka^{-1} internal alpha dose rate (Bowler *et al.*, 2003).
6. Mean ± standard (1σ) error, where the error includes a 2% uncertainty associated with calibration of the laboratory beta source.
7. Age model used to determine the paleodose, where CAM and MAM are the central age and minimum age model (Galbraith *et al.* 1999), respectively. All samples designated MAM were analyzed using the three-parameter minimum age model; prior to running the model, an additional of 10% overdispersion was added in quadrature to the measurement uncertainty for each of the single-grain paleodoses.
8. Paleodose overdispersion (i.e. the spread in paleodose values after taking all measurement uncertainties into account).
9. Mean ± total (1σ) uncertainty, calculated as the quadratic sum of the random and systematic uncertainties.
10. KY3 was reported as 46 ± 2 ka (megafaunal unit, pit 2) in Roberts *et al.* (2001), based on the analysis of multi-grain aliquots. The same sample has been re-dated in this study using single-grain measurements, which we consider more accurate.

Table S3. $^{230}Th/^{234}U$ ages for samples of flowstone interbedded with fossil-bearing sediments in Tight Entrance Cave.

Sample	Lab no. and Date	U(ngg^{-1})	$[^{230}Th/^{238}U]^a$	$[^{234}U/^{238}U]^a$	$[^{232}Th/^{238}U]$	$[^{230}Th/^{232}Th]$	$[^{234}U/^{238}U]_i^b$	Age (ka)[c]
WAM 07.6.147 TEC-F unit G	UMA01786 Sep-2007	18	0.395(07)	1.090(08)	0.149(.002)	2.64	1.102(09)	44.9 ± 1.3
TEC-F unit G lower	UMA01788 Sep-2007	18	0.411(18)	1.083(11)	0.114(.001)	3.60	1.095(12)	48.7 ± 3.0
TEC-F N.E. Face unit D	UMA01789 Sep-2007	33	0.747(28)	1.054(18)	0.734(.013)	1.02	1.074(24)	112 ± 11
TEC-K-D2 unit D	UMA03013 Nov-2009	38	0.824(17)	1.053(06)	0.583(.025)	1.41	1.081(08)	146.3 ± 8.4
TEC-97 unit B	UMA03017 Nov-2009	28	0.889(14)	1.055(06)	1.430(.044)	0.62	1.084(09)	151 ± 13

[a] Activity ratios determined after Hellstrom (2003) using the decay constants of Cheng *et al.* (2000)

[b] Initial $[^{234}U/^{238}U]$ calculated using corrected age

[c] Age corrected for initial ^{230}Th using equation 1 of Hellstrom (2006), $[^{230}Th/^{232}Th]_i$ of 0.245 ± 0.035 and the decay constants of Cheng *et al.* (2000). Errors reported at 1σ.

Uranium-Thorium Dating

$^{230}Th/^{234}U$ dating was conducted on solid pieces of calcite of approximately 30 mg, cut from the speleothem samples using a dental drill. Samples were dissolved in nitric acid and equilibrated with a mixed ^{229}Th–^{233}U tracer. U and Th were extracted using Eichrom TRU resin before introduction to a Nu Plasma MC-ICP-MS where isotope ratios of both elements were measured simultaneously (Hellstrom 2003). A well-constrained initial [$^{230}Th/^{232}Th$] of 0.245 ± 0.035 was determined and its uncertainty fully propagated (Hellstrom 2006).

Table S4. Summary of Tight Entrance Cave chronology.

Unit	^{14}C (cal ka)[1]	$^{230}Th/^{234}U$ (ka)[1]	Optical (ka)[1]
J	29.1 ± 0.3		33 ± 3
H	34.6 ± 0.4		32 ± 3
	37 ± 1		34 ± 2
G	48 ± 1	44 ± 2	43 ± 4[2]
		44.9 ± 0.7	
		47 ± 1	
		49 ± 2	
		49 ± 3	
F2	47 ± 2		47 ± 3
F1			45 ± 4
			53 ± 4
E	51 ± 2		
E*			70 ± 4
D	>62	112 ± 6	89 ± 6
		119 ± 4	95 ± 7
			98 ± 8
			103 ± 7
		137 ± 3[3]	136 ± 22[4]
		146 ± 4[5]	
B		151 ± 7	135 ± 7
A			227 ± 13

1. Errors are reported at 1σ.
2. This sample was mistakenly ascribed to unit H in Ayliffe *et al.* (2008).
3. This sample was collected from a flowstone revealed by excavation in 2008 to be on the boundary of units B and D (cf. Prideaux 1999; Ayliffe *et al.* 2008).
4. This sample was collected immediately beneath the 137 ± 3 ka flowstone and therefore pertains to the top of unit B.
5. The flowstone from which this sample was taken was rotated 90° (oriented vertically) and thus not in primary position. Its age is therefore provides only an absolute maximum for unit D and was more likely formed at around the same time as the small *in situ* flowstone providing the sample dated to 151 ± 13 ka.

STABLE ISOTOPE ANALYSIS OF LAND-SNAIL SHELLS

Background

Land snails precipitate aragonitic shells in isotopic equilibrium with the bicarbonate pool of body waters. Stable carbon and oxygen isotope compositions of respired CO_2 and body water, which determine $\delta^{13}C$ and $\delta^{18}O$ of the bicarbonate pool, appear in turn to be influenced by a variety of external environmental parameters (Goodfriend *et al.* 1989). Precise relationships governing land-snail shell stable isotopes and environmental conditions has been the subject of considerable debate over the years. While land-snail shell carbon isotopes are regarded by the majority to be related to those of snail diet (usually comprised of local vegetation with minor contributions from limestone substrates (Francey 1983; Goodfriend and Hood 1983; Goodfriend *et al.* 1989), the factors determining land-snail shell oxygen isotopes appear much more complicated. Previous empirical studies of modern land snails have shown $\delta^{18}O$ values of shell aragonite ($\delta^{18}O_{shell}$) to be related to rainfall $\delta^{18}O$ values ($\delta^{18}O_{rain}$), and in arid environments, also to relative humidity (h) (Yapp 1979; Margaritz *et al.* 1981; Goodfriend *et al.* 1989; Balakrishnan *et al.* 2005). In addition to this, Balakrishnan and Yapp (2004) find stable isotopes of land-snail shells are also influenced by temperature, the $\delta^{18}O$ of ambient water vapor and snail physiologies.

Sampling and cleaning protocols

Thirty-one modern and fossil land snail (*Bothriembryon sayi)* shells from the Tight Entrance Cave deposit and environs were serially sampled and analysed for stable isotopes. The state of preservation of the fossil land snails appeared exceptional, with no signs of recrystallization of the primary aragonite tests to calcite (Couzens 2007). Shells were cleaned by first soaking overnight in 3% H_2O_2 to remove organics. The H_2O_2 reagent was then changed, and shells placed in an ultrasonic bath for three 10-minute sessions prior to rinsing several times in demineralized water. Cleaned shells were then dried overnight at 60°C.

Shells of similar size (Table S5) were preferentially selected for analysis in order to minimize any inter-shell variations arising from differential calcification stages. Land-snail shell calcification is known to take place in several stages, an initial protoconch phase formed within the egg capsule, a rapid growth/extension phase and a subsequent shell thickening stage after shells have reached maturity (Cowie, 1984). Small segments (~0.5 x 1.5 x 4 mm) were cut from 25 sequential layers perpendicular to the spiraled shell growth axis (Fig. S6) using a small diamond-impregnated grinding wheel. After sectioning, adhering secondary calcite overgrowths (present on many of the fossil land-snail shells) were removed mechanically using a small scalpel blade. This procedure was deemed necessary as the calcite matrix from one heavily calcified specimen from Unit D (TEC-

99,D,S-1mtx) had a very different isotope composition to the shell it coated (Table S5). Every third segment was then crushed to a fine powder prior to mass spectrometric analysis.

Powdered shell samples (~200µg) were reacted at 90°C in a Kiel carbonate device and analysed on a Finnigan MAT251 mass spectrometer. Isotope results were standardised to the Vienna-Peedee Belemnite (V-PDB) scale by in-run comparison to NBS-19 and NBS-18. $\delta^{13}C$, $\delta^{18}O$ ‰ = [(Rsample / Rstandard) –1] x 1000, where R is the $^{13}C/^{12}C$ or $^{18}O/^{16}O$ ratio. Reproducibility of $\delta^{13}C$ and $\delta^{18}O$ for NBS-19 (n=80) during the period of analysis was ± 0.02 (1σ)‰ and ± 0.03‰, respectively.

Figure S6. Examples of sectioning land-snail samples from TEC for stable isotope analysis.

By choosing shells that were about three-quarters of the size of fully mature specimens, and still in the rapid growth phase, it was hoped that any affects associated with a two stage calcification process (i.e. shell extension followed by thickening), which would smooth isotopic signatures, might be minimized. In practice it appeared some degree of smoothing related to shell thickening was unavoidable as the sectioned segments were observed under the microscope to be comprised of an outer layer produced from shell extension and a (usually thinner) inner layer surmised to be associated with shell thickening. Separating these two layers prior to isotope analysis was not feasible for this study due to physical limitations in handling sub-millimeter sized material.

Despite these likely smoothing effects the majority of the stable isotope records generated in this study using this sampling protocol exhibit stable isotope patterns between 3/4 and 1 1/4 isotope (presumably annual) cycles in length (Table S5, Fig. S8). From these records it should therefore be possible to derive reasonable estimates of the average shell $\delta^{13}C$ and $\delta^{18}O$ values acquired during periods of land-snail activity in a given year.

Table S5. Raw stable carbon- and oxygen-isotope data ($\delta^{13}C$, $\delta^{18}O$) from the shells of modern and fossil land snails (*Bothriembryon sayi*) utilized in this study.

sample ID	Sample Type	Shell length (mm)	Shell width (mm)	Unit/Age	Sub-sample No.	$\delta^{13}C$ V-PDB (‰)	$\delta^{18}O$ V-PDB (‰)
TEC,Liv.,S-1-1	Land-snail Shells	10.7	20.7	Modern	1	-10.83	-0.14
TEC,Liv.,S-1-4	Land-snail Shells	10.7	20.7	Modern	4	-11.26	-0.87
TEC,Liv.,S-1-7	Land-snail Shells	10.7	20.7	Modern	7	-11.42	-1.23
TEC,Liv.,S-1-10	Land-snail Shells	10.7	20.7	Modern	10	-11.38	-1.20
TEC,Liv.,S-1-13	Land-snail Shells	10.7	20.7	Modern	13	-11.41	-1.15
TEC,Liv.,S-1-16	Land-snail Shells	10.7	20.7	Modern	16	-11.35	-1.13
TEC,Liv.,S-1-19	Land-snail Shells	10.7	20.7	Modern	19	-11.12	-0.96
TEC,Liv.,S-1-22	Land-snail Shells	10.7	20.7	Modern	22	-11.03	-0.62
TEC,Liv.,S-1-25	Land-snail Shells	10.7	20.7	Modern	25	-10.95	-0.71
TEC,Mod.,S-2-1	Land-snail Shells	11.2	23.7	Modern	1	-10.44	-0.83
TEC,Mod.,S-2-4	Land-snail Shells	11.2	23.7	Modern	4	-10.78	-0.79
TEC,Mod.,S-2-7	Land-snail Shells	11.2	23.7	Modern	7	-11.49	-0.65
TEC,Mod.,S-2-10	Land-snail Shells	11.2	23.7	Modern	10	-11.03	-0.36
TEC,Mod.,S-2-13	Land-snail Shells	11.2	23.7	Modern	13	-10.84	-0.54
TEC,Mod.,S-2-16	Land-snail Shells	11.2	23.7	Modern	16	-11.39	-0.35
TEC,Mod.,S-2-19	Land-snail Shells	11.2	23.7	Modern	19	-11.62	-0.31
TEC,Mod.,S-2-22	Land-snail Shells	11.2	23.7	Modern	22	-11.40	-0.40
TEC,Mod.,S-2-25	Land-snail Shells	11.2	23.7	Modern	25	-11.14	-0.30
TEC,Rec.,S-1-1	Land-snail Shells	10.4	23.8	Modern	1	-10.05	-0.48
TEC,Rec.,S-1-4	Land-snail Shells	10.4	23.8	Modern	4	-10.24	-1.11
TEC,Rec.,S-1-7	Land-snail Shells	10.4	23.8	Modern	7	-10.33	-0.94
TEC,Rec.,S-1-10	Land-snail Shells	10.4	23.8	Modern	10	-10.46	-0.61
TEC,Rec.,S-1-13	Land-snail Shells	10.4	23.8	Modern	13	-10.00	0.00
TEC,Rec.,S-1-16	Land-snail Shells	10.4	23.8	Modern	16	-9.96	-0.39
TEC,Rec.,S-1-19	Land-snail Shells	10.4	23.8	Modern	19	-9.81	-0.78
TEC,Rec.,S-1-22	Land-snail Shells	10.4	23.8	Modern	22	-9.63	-0.74
TEC,Rec.,S-1-25	Land-snail Shells	10.4	23.8	Modern	25	-9.72	-0.56
TEC,Rec.,S-2-1	Land-snail Shells	11.5	24.2	Modern	1	-9.21	-0.52
TEC,Rec.,S-2-4	Land-snail Shells	11.5	24.2	Modern	4	-9.38	-0.25
TEC,Rec.,S-2-7	Land-snail Shells	11.5	24.2	Modern	7	-9.13	-0.38
TEC,Rec.,S-2-10	Land-snail Shells	11.5	24.2	Modern	10	-9.01	-0.45
TEC,Rec.,S-2-13	Land-snail Shells	11.5	24.2	Modern	13	-9.14	-0.53
TEC,Rec.,S-2-16	Land-snail Shells	11.5	24.2	Modern	16	-8.68	-0.43
TEC,Rec.,S-2-19	Land-snail Shells	11.5	24.2	Modern	19	-9.41	0.20
TEC,Rec.,S-2-22	Land-snail Shells	11.5	24.2	Modern	22	-9.34	-0.50
TEC,Rec.,S-2-25	Land-snail Shells	11.5	24.2	Modern	25	-10.39	-0.18
TEC-E,J,S-1-1	Land-snail Shells	n.d.	n.d.	Unit J	1	-7.73	-1.27
TEC-E,J,S-1-4	Land-snail Shells	n.d.	n.d.	Unit J	4	-7.97	0.75
TEC-E,J,S-1-7	Land-snail Shells	n.d.	n.d.	Unit J	7	-7.12	0.83
TEC-E,J,S-1-10	Land-snail Shells	n.d.	n.d.	Unit J	10	-7.13	1.25
TEC-E,J,S-1-13	Land-snail Shells	n.d.	n.d.	Unit J	13	-7.33	1.03

TEC-E,J,S-1-16	Land-snail Shells	n.d.	n.d.	Unit J	16	-7.46	0.25
TEC-E,J,S-1-19	Land-snail Shells	n.d.	n.d.	Unit J	19	-7.33	-0.06
TEC-E,J,S-1-22	Land-snail Shells	n.d.	n.d.	Unit J	22	-6.86	2.21
TEC-E,J,S-1-25	Land-snail Shells	n.d.	n.d.	Unit J	25	-4.93	1.21
TEC-E,J,S-2-1	Land-snail Shells	n.d.	n.d.	Unit J	1	-7.67	1.43
TEC-E,J,S-2-4	Land-snail Shells	n.d.	n.d.	Unit J	4	-7.56	0.97
TEC-E,J,S-2-7	Land-snail Shells	n.d.	n.d.	Unit J	7	-6.44	0.34
TEC-E,J,S-2-10	Land-snail Shells	n.d.	n.d.	Unit J	10	-6.46	-0.06
TEC-E,J,S-2-13	Land-snail Shells	n.d.	n.d.	Unit J	13	-7.59	-0.24
TEC-E,J,S-2-16	Land-snail Shells	n.d.	n.d.	Unit J	16	-7.66	0.33
TEC-E,J,S-2-19	Land-snail Shells	n.d.	n.d.	Unit J	19	-5.58	0.43
TEC-E,J,S-2-22	Land-snail Shells	n.d.	n.d.	Unit J	22	-6.68	-0.31
TEC-E,J,S-2-25	Land-snail Shells	n.d.	n.d.	Unit J	25	-6.95	0.88
TEC-E,J,S-3-1	Land-snail Shells	11.2	23.1	Unit J	1	-9.76	-0.12
TEC-E,J,S-3-4	Land-snail Shells	11.2	23.1	Unit J	4	-7.99	-0.10
TEC-E,J,S-3-7	Land-snail Shells	11.2	23.1	Unit J	7	-7.90	-0.30
TEC-E,J,S-3-10	Land-snail Shells	11.2	23.1	Unit J	10	-6.87	-1.03
TEC-E,J,S-3-13	Land-snail Shells	11.2	23.1	Unit J	13	-7.18	-0.03
TEC-E,J,S-3-16	Land-snail Shells	11.2	23.1	Unit J	16	-7.64	0.36
TEC-E,J,S-3-19	Land-snail Shells	11.2	23.1	Unit J	19	-7.55	0.69
TEC-E,J,S-3-22	Land-snail Shells	11.2	23.1	Unit J	22	-7.55	0.14
TEC-E,J,S-3-25	Land-snail Shells	11.2	23.1	Unit J	25	-7.17	0.30
TEC,J,S5-1	Land-snail Shells	10.6	22.0	Unit J	1	-8.08	-0.40
TEC,J,S5-4	Land-snail Shells	10.6	22.0	Unit J	4	-7.83	-0.08
TEC,J,S5-7	Land-snail Shells	10.6	22.0	Unit J	7	-7.78	0.86
TEC,J,S5-10	Land-snail Shells	10.6	22.0	Unit J	10	-5.77	-1.34
TEC,J,S5-13	Land-snail Shells	10.6	22.0	Unit J	13	-5.64	-0.75
TEC,J,S5-16	Land-snail Shells	10.6	22.0	Unit J	16	-5.24	-0.39
TEC,J,S5-19	Land-snail Shells	10.6	22.0	Unit J	19	-4.68	-0.16
TEC,J,S5-22	Land-snail Shells	10.6	22.0	Unit J	22	-4.59	0.71
TEC,J,S5-25	Land-snail Shells	10.6	22.0	Unit J	25	-4.73	0.35
TEC-E-S4-1	Land-snail Shells	10.7	23.5	Unit J	1	-7.48	0.04
TEC-E-S4-4	Land-snail Shells	10.7	23.5	Unit J	4	-7.48	0.47
TEC-E-S4-7	Land-snail Shells	10.7	23.5	Unit J	7	-7.19	0.53
TEC-E-S4-10	Land-snail Shells	10.7	23.5	Unit J	10	-6.43	0.62
TEC-E-S4-13	Land-snail Shells	10.7	23.5	Unit J	13	-5.28	-0.25
TEC-E-S4-16	Land-snail Shells	10.7	23.5	Unit J	16	-5.58	-0.42
TEC-E-S4-19	Land-snail Shells	10.7	23.5	Unit J	19	-6.48	-0.38
TEC-E-S4-22	Land-snail Shells	10.7	23.5	Unit J	22	-5.77	-0.09
TEC-E-S4-25	Land-snail Shells	10.7	23.5	Unit J	25	-6.32	-0.37
TEC-D,H,S-1-1	Land-snail Shells	11.2	23.6	Unit H	1	-8.47	-0.09
TEC-D,H,S-1-4	Land-snail Shells	11.2	23.6	Unit H	4	-8.02	0.62
TEC-D,H,S-1-7	Land-snail Shells	11.2	23.6	Unit H	7	-7.99	0.31
TEC-D,H,S-1-10	Land-snail Shells	11.2	23.6	Unit H	10	-7.74	0.07
TEC-D,H,S-1-13	Land-snail Shells	11.2	23.6	Unit H	13	-7.32	-0.08
TEC-D,H,S-1-16	Land-snail Shells	11.2	23.6	Unit H	16	-7.04	0.51
TEC-D,H,S-1-19	Land-snail Shells	11.2	23.6	Unit H	19	-6.84	0.49

TEC-D,H,S-1-22	Land-snail Shells	11.2	23.6	Unit H	22	-6.85	0.58
TEC-D,H,S-1-25	Land-snail Shells	11.2	23.6	Unit H	25	-7.38	-0.41
TEC-D,H,S-2-1	Land-snail Shells	11.4	24.0	Unit H	1	-8.13	-1.58
TEC-D,H,S-2-4	Land-snail Shells	11.4	24.0	Unit H	4	-7.68	-1.56
TEC-D,H,S-2-7	Land-snail Shells	11.4	24.0	Unit H	7	-8.15	-1.41
TEC-D,H,S-2-10	Land-snail Shells	11.4	24.0	Unit H	10	-8.02	-0.39
TEC-D,H,S-2-13	Land-snail Shells	11.4	24.0	Unit H	13	-8.70	-0.64
TEC-D,H,S-2-16	Land-snail Shells	11.4	24.0	Unit H	16	-8.46	-1.28
TEC-D,H,S-2-19	Land-snail Shells	11.4	24.0	Unit H	19	-8.47	-1.16
TEC-D,H,S-2-22	Land-snail Shells	11.4	24.0	Unit H	22	-8.53	-0.27
TEC-D,H,S-2-25	Land-snail Shells	11.4	24.0	Unit H	25	-7.40	0.62
TEC-G,H,S-3-1	Land-snail Shells	11.8	24.8	Unit H	1	-7.75	-0.48
TEC-G,H,S-3-4	Land-snail Shells	11.8	24.8	Unit H	4	-8.01	-0.70
TEC-G,H,S-3-7	Land-snail Shells	11.8	24.8	Unit H	7	-8.38	-0.24
TEC-G,H,S-3-10	Land-snail Shells	11.8	24.8	Unit H	10	-6.90	0.23
TEC-G,H,S-3-13	Land-snail Shells	11.8	24.8	Unit H	13	-6.52	-0.76
TEC-G,H,S-3-16	Land-snail Shells	11.8	24.8	Unit H	16	-6.57	-0.74
TEC-G,H,S-3-19	Land-snail Shells	11.8	24.8	Unit H	19	-6.44	0.04
TEC-G,H,S-3-22	Land-snail Shells	11.8	24.8	Unit H	22	-6.69	-0.57
TEC-G,H,S-3-25	Land-snail Shells	11.8	24.8	Unit H	25	-6.69	0.07
TEC-H,F2,S-1-1	Land-snail Shells	11.3	21.5	Unit F2	1	-11.37	-0.94
TEC-H,F2,S-1-4	Land-snail Shells	11.3	21.5	Unit F2	4	-10.75	-1.29
TEC-H,F2,S-1-7	Land-snail Shells	11.3	21.5	Unit F2	7	-11.05	-1.69
TEC-H,F2,S-1-10	Land-snail Shells	11.3	21.5	Unit F2	10	-11.86	-1.45
TEC-H,F2,S-1-13	Land-snail Shells	11.3	21.5	Unit F2	13	-11.87	-0.39
TEC-H,F2,S-1-16	Land-snail Shells	11.3	21.5	Unit F2	16	-12.04	-1.40
TEC-H,F2,S-1-19	Land-snail Shells	11.3	21.5	Unit F2	19	-13.14	-1.99
TEC-H,F2,S-1-22	Land-snail Shells	11.3	21.5	Unit F2	22	-12.77	-1.73
TEC-H,F2,S-1-25	Land-snail Shells	11.3	21.5	Unit F2	25	-11.97	-1.01
TEC-H,F2,S-2-1	Land-snail Shells	9.8	20.3	Unit F2	1	-7.39	-0.45
TEC-H,F2,S-2-4	Land-snail Shells	9.8	20.3	Unit F2	4	-6.72	-0.49
TEC-H,F2,S-2-7	Land-snail Shells	9.8	20.3	Unit F2	7	-7.02	-0.90
TEC-H,F2,S-2-10	Land-snail Shells	9.8	20.3	Unit F2	10	-7.46	-0.55
TEC-H,F2,S-2-13	Land-snail Shells	9.8	20.3	Unit F2	13	-7.62	-0.69
TEC-H,F2,S-2-16	Land-snail Shells	9.8	20.3	Unit F2	16	-7.58	-0.31
TEC-H,F2,S-2-19	Land-snail Shells	9.8	20.3	Unit F2	19	-6.80	-0.57
TEC-H,F2,S-2-22	Land-snail Shells	9.8	20.3	Unit F2	22	-7.25	-0.34
TEC-H,F2,S-2-25	Land-snail Shells	9.8	20.3	Unit F2	25	-6.43	0.11
TEC-H,F2,S-4-1	Land-snail Shells	10.0	21.8†	Unit F2	1	-7.19	-1.03
TEC-H,F2,S-4-4	Land-snail Shells	10.0	21.8†	Unit F2	4	-7.49	-0.63
TEC-H,F2,S-4-7	Land-snail Shells	10.0	21.8†	Unit F2	7	-7.76	-0.86
TEC-H,F2,S-4-10	Land-snail Shells	10.0	21.8†	Unit F2	10	-7.57	-1.71
TEC-H,F2,S-4-13	Land-snail Shells	10.0	21.8†	Unit F2	13	-7.89	-1.81
TEC-H,F2,S-4-16	Land-snail Shells	10.0	21.8†	Unit F2	16	-8.31	-1.08
TEC-H,F2,S-4-19	Land-snail Shells	10.0	21.8†	Unit F2	19	-7.44	-0.04
TEC-H,F2,S-4-22	Land-snail Shells	10.0	21.8†	Unit F2	22	-7.89	-0.64
TEC-H,F2,S-4-25	Land-snail Shells	10.0	21.8†	Unit F2	25	-8.03	-0.31

TEC-E,F2,S-5-2	Land-snail Shells	9.5	21.0†	Unit F2	2	-9.24	-0.34
TEC-E,F2,S-5-5	Land-snail Shells	10.5	21.0†	Unit F2	5	-9.41	1.08
TEC-E,F2,S-5-8	Land-snail Shells	11.5	21.0†	Unit F2	8	-9.06	-0.26
TEC-E,F2,S-5-11	Land-snail Shells	12.5	21.0†	Unit F2	11	-9.31	-0.13
TEC-E,F2,S-5-14	Land-snail Shells	13.5	21.0†	Unit F2	14	-9.69	0.50
TEC-E,F2,S-5-17	Land-snail Shells	14.5	21.0†	Unit F2	17	-10.20	-0.82
TEC-E,F2,S-5-20	Land-snail Shells	15.5	21.0†	Unit F2	20	-10.80	-0.25
TEC-E,F2,S-5-23	Land-snail Shells	16.5	21.0†	Unit F2	23	-10.84	0.26
TEC-E,F2,S-5-26	Land-snail Shells	17.5	21.0†	Unit F2	26	-10.58	0.22
TEC-H,F1,S-1-1	Land-snail Shells	10.3	21.8	Unit F1	1	-8.65	-0.60
TEC-H,F1,S-1-4	Land-snail Shells	10.3	21.8	Unit F1	4	-9.09	-1.38
TEC-H,F1,S-1-7	Land-snail Shells	10.3	21.8	Unit F1	7	-9.11	-1.21
TEC-H,F1,S-1-10	Land-snail Shells	10.3	21.8	Unit F1	10	-9.97	-0.51
TEC-H,F1,S-1-13	Land-snail Shells	10.3	21.8	Unit F1	13	-9.73	-0.81
TEC-H,F1,S-1-16	Land-snail Shells	10.3	21.8	Unit F1	16	-10.09	-0.06
TEC-H,F1,S-1-19	Land-snail Shells	10.3	21.8	Unit F1	19	-10.26	0.55
TEC-H,F1,S-1-22	Land-snail Shells	10.3	21.8	Unit F1	22	-9.67	0.24
TEC-H,F1,S-1-25	Land-snail Shells	10.3	21.8	Unit F1	25	-9.37	-0.11
TEC-H,F1,S-2-1	Land-snail Shells	10.4	20†	Unit F1	1	-8.45	-1.43
TEC-H,F1,S-2-4	Land-snail Shells	10.4	20†	Unit F1	4	-6.81	0.21
TEC-H,F1,S-2-7	Land-snail Shells	10.4	20†	Unit F1	7	-6.06	-0.07
TEC-H,F1,S-2-10	Land-snail Shells	10.4	20†	Unit F1	10	-6.45	0.61
TEC-H,F1,S-2-13	Land-snail Shells	10.4	20†	Unit F1	13	-6.41	0.50
TEC-H,F1,S-2-16	Land-snail Shells	10.4	20†	Unit F1	16	-6.29	0.84
TEC-H,F1,S-2-19	Land-snail Shells	10.4	20†	Unit F1	19	-6.80	0.87
TEC-H,F1,S-2-22	Land-snail Shells	10.4	20†	Unit F1	22	-6.89	1.03
TEC-H,F1,S-2-25	Land-snail Shells	10.4	20†	Unit F1	25	-6.72	1.22
TEC-K,F1,S-3-1	Land-snail Shells	9.4	21.9	Unit F1	1	-8.54	-1.60
TEC-K,F1,S-3-4	Land-snail Shells	9.4	21.9	Unit F1	4	-8.49	-1.63
TEC-K,F1,S-3-7	Land-snail Shells	9.4	21.9	Unit F1	7	-7.95	-1.16
TEC-K,F1,S-3-10	Land-snail Shells	9.4	21.9	Unit F1	10	-8.20	-0.99
TEC-K,F1,S-3-13	Land-snail Shells	9.4	21.9	Unit F1	13	-8.30	0.30
TEC-K,F1,S-3-16	Land-snail Shells	9.4	21.9	Unit F1	16	-7.85	-0.52
TEC-K,F1,S-3-19	Land-snail Shells	9.4	21.9	Unit F1	19	-8.48	-0.63
TEC-K,F1,S-3-22	Land-snail Shells	9.4	21.9	Unit F1	22	-7.01	-1.01
TEC-K,F1,S-3-25	Land-snail Shells	9.4	21.9	Unit F1	25	-7.41	-0.60
TEC-E,E*,S-1-1	Land-snail Shells	10.4	21.0	Unit E*	1	-10.47	-1.50
TEC-E,E*,S-1-4	Land-snail Shells	10.4	21.0	Unit E*	4	-10.46	-1.44
TEC-E,E*,S-1-7	Land-snail Shells	10.4	21.0	Unit E*	7	-10.40	-1.88
TEC-E,E*,S-1-10	Land-snail Shells	10.4	21.0	Unit E*	10	-10.82	-0.64
TEC-E,E*,S-1-13	Land-snail Shells	10.4	21.0	Unit E*	13	-11.64	-0.73
TEC-E,E*,S-1-16	Land-snail Shells	10.4	21.0	Unit E*	16	-12.63	-1.47
TEC-E,E*,S-1-19	Land-snail Shells	10.4	21.0	Unit E*	19	-12.52	-0.02
TEC-E,E*,S-1-22	Land-snail Shells	10.4	21.0	Unit E*	22	-12.38	-1.13
TEC-E,E*,S-1-25	Land-snail Shells	10.4	21.0	Unit E*	25	-12.52	-1.33
TEC-E,E*,S-2-1	Land-snail Shells	10.0	20.4	Unit E*	1	-10.54	-1.56
TEC-E,E*,S-2-4	Land-snail Shells	10.0	20.4	Unit E*	4	-9.97	-1.46

TEC-E,E*,S-2-7	Land-snail Shells	10.0	20.4	Unit E*	7	-10.49	-2.25
TEC-E,E*,S-2-10	Land-snail Shells	10.0	20.4	Unit E*	10	-10.53	-1.45
TEC-E,E*,S-2-13	Land-snail Shells	10.0	20.4	Unit E*	13	-11.13	-1.54
TEC-E,E*,S-2-16	Land-snail Shells	10.0	20.4	Unit E*	16	-11.14	-1.65
TEC-E,E*,S-2-19	Land-snail Shells	10.0	20.4	Unit E*	19	-10.77	-1.37
TEC-E,E*,S-2-22	Land-snail Shells	10.0	20.4	Unit E*	22	-11.03	-1.34
TEC-E,E*,S-2-25	Land-snail Shells	10.0	20.4	Unit E*	25	-10.95	-1.28
TEC-M,E*,S-3-2	Land-snail Shells	10.4	22.1	Unit E*	2	-7.64	-1.85
TEC-M,E*,S-3-5	Land-snail Shells	10.4	22.1	Unit E*	5	-8.19	-0.42
TEC-M,E*,S-3-8	Land-snail Shells	10.4	22.1	Unit E*	8	-7.36	0.01
TEC-M,E*,S-3-11	Land-snail Shells	10.4	22.1	Unit E*	11	-7.76	-0.97
TEC-M,E*,S-3-14	Land-snail Shells	10.4	22.1	Unit E*	14	-6.82	-0.79
TEC-M,E*,S-3-17	Land-snail Shells	10.4	22.1	Unit E*	17	-6.71	-1.54
TEC-M,E*,S-3-20	Land-snail Shells	10.4	22.1	Unit E*	20	-6.65	-0.99
TEC-M,E*,S-3-23	Land-snail Shells	10.4	22.1	Unit E*	23	-7.24	-0.16
TEC-M,E*,S-3-26	Land-snail Shells	10.4	22.1	Unit E*	26	-7.37	-0.80
TEC-K,D2,S-1-1	Land-snail Shells	11.0	24.0	Unit D	1	-13.97	-1.09
TEC-K,D2,S-1-4	Land-snail Shells	11.0	24.0	Unit D	4	-14.50	-0.52
TEC-K,D2,S-1-7	Land-snail Shells	11.0	24.0	Unit D	7	-14.64	-0.88
TEC-K,D2,S-1-10	Land-snail Shells	11.0	24.0	Unit D	10	-14.33	-0.82
TEC-K,D2,S-1-13	Land-snail Shells	11.0	24.0	Unit D	13	-14.04	-0.57
TEC-K,D2,S-1-16	Land-snail Shells	11.0	24.0	Unit D	16	-13.56	-0.89
TEC-K,D2,S-1-19	Land-snail Shells	11.0	24.0	Unit D	19	-13.73	-1.31
TEC-K,D2,S-1-22	Land-snail Shells	11.0	24.0	Unit D	22	-13.61	-0.66
TEC-K,D2,S-1-25	Land-snail Shells	11.0	24.0	Unit D	25	-13.84	-0.34
TEC-H,D2,S-2-1	Land-snail Shells	10.7	23.6	Unit D	1	-10.49	-0.91
TEC-H,D2,S-2-4	Land-snail Shells	10.7	23.6	Unit D	4	-10.77	-1.58
TEC-H,D2,S-2-7	Land-snail Shells	10.7	23.6	Unit D	7	-10.69	-1.57
TEC-H,D2,S-2-10	Land-snail Shells	10.7	23.6	Unit D	10	-11.07	-1.76
TEC-H,D2,S-2-13	Land-snail Shells	10.7	23.6	Unit D	13	-10.86	-1.20
TEC-H,D2,S-2-16	Land-snail Shells	10.7	23.6	Unit D	16	-10.62	-1.24
TEC-H,D2,S-2-19	Land-snail Shells	10.7	23.6	Unit D	19	-10.54	-1.11
TEC-N,D2,S-2-22	Land-snail Shells	10.7	23.6	Unit D	22	-10.58	-0.77
TEC-N,D2,S-2-25	Land-snail Shells	10.7	23.6	Unit D	25	-10.91	-0.45
TEC-H,D2,S-3-1	Land-snail Shells	10.2	20.0	Unit D	1	-10.66	-2.01
TEC-H,D2,S-3-4	Land-snail Shells	10.2	20.0	Unit D	4	-10.69	-1.68
TEC-H,D2,S-3-7	Land-snail Shells	10.2	20.0	Unit D	7	-10.65	-1.78
TEC-H,D2,S-3-10	Land-snail Shells	10.2	20.0	Unit D	10	-10.52	-0.90
TEC-H,D2,S-3-13	Land-snail Shells	10.2	20.0	Unit D	13	-10.83	-0.84
TEC-H,D2,S-3-16	Land-snail Shells	10.2	20.0	Unit D	16	-11.04	-0.51
TEC-H,D2,S-3-19	Land-snail Shells	10.2	20.0	Unit D	19	-11.11	0.14
TEC-H,D2,S-3-22	Land-snail Shells	10.2	20.0	Unit D	22	-11.26	-0.32
TEC-H,D2,S-3-25	Land-snail Shells	10.2	20.0	Unit D	25	-10.64	-0.88
TEC-99,D,S-1mtx	Matrix Calcite	n.a.	n.a.	Unit D		-10.93	-4.07
TEC-99,D,S-1-1	Land-snail Shells	10.6	21.6	Unit D	1	-10.11	-1.43
TEC-99,D,S-1-4	Land-snail Shells	10.6	21.6	Unit D	4	-10.71	-0.91
TEC-99,D,S-1-7	Land-snail Shells	10.6	21.6	Unit D	7	-10.54	-1.08

TEC-99,D,S-1-10	Land-snail Shells	10.6	21.6	Unit D	10	-10.32	-0.62
TEC-99,D,S-1-13	Land-snail Shells	10.6	21.6	Unit D	13	-10.57	-1.07
TEC-99,D,S-1-16	Land-snail Shells	10.6	21.6	Unit D	16	-10.66	-1.09
TEC-99,D,S-1-19	Land-snail Shells	10.6	21.6	Unit D	19	-10.36	-1.33
TEC-99,D,S-1-22	Land-snail Shells	10.6	21.6	Unit D	22	-10.34	-1.54
TEC-99,D,S-1-25	Land-snail Shells	10.6	21.6	Unit D	25	-10.56	-1.25
TEC-99,D,S-2-1	Land-snail Shells	11.2	24.2	Unit D	1	-9.23	-1.44
TEC-99,D,S-2-4	Land-snail Shells	11.2	24.2	Unit D	4	-10.29	-1.69
TEC-99,D,S-2-7	Land-snail Shells	11.2	24.2	Unit D	7	-10.24	-1.57
TEC-99,D,S-2-10	Land-snail Shells	11.2	24.2	Unit D	10	-10.41	-1.34
TEC-99,D,S-2-13	Land-snail Shells	11.2	24.2	Unit D	13	-10.88	-1.02
TEC-99,D,S-2-16	Land-snail Shells	11.2	24.2	Unit D	16	-10.96	-1.56
TEC-99,D,S-2-19	Land-snail Shells	11.2	24.2	Unit D	19	-11.04	-1.25
TEC-99,D,S-2-22	Land-snail Shells	11.2	24.2	Unit D	22	-11.56	-1.64
TEC-99,D,S-2-25	Land-snail Shells	11.2	24.2	Unit D	25	-11.50	-1.95
TEC-99,D,S-3-1	Land-snail Shells	10.0	21.2	Unit D	1	-10.42	-1.59
TEC-99,D,S-3-4	Land-snail Shells	10.0	21.2	Unit D	4	-11.03	-1.46
TEC-99,D,S-3-7	Land-snail Shells	10.0	21.2	Unit D	7	-11.17	-1.35
TEC-99,D,S-3-10	Land-snail Shells	10.0	21.2	Unit D	10	-11.21	-0.45
TEC-99,D,S-3-13	Land-snail Shells	10.0	21.2	Unit D	13	-11.72	-0.95
TEC-99,D,S-3-16	Land-snail Shells	10.0	21.2	Unit D	16	-12.28	-0.98
TEC-99,D,S-3-19	Land-snail Shells	10.0	21.2	Unit D	19	-11.39	-0.95
TEC-99,D,S-3-22	Land-snail Shells	10.0	21.2	Unit D	22	-11.78	-1.12
TEC-99,D,S-3-25	Land-snail Shells	10.0	21.2	Unit D	25	-11.66	-1.05
TEC,B,S-1-1	Land-snail Shells	10.1	19.3	Unit B	1	-7.56	-0.47
TEC,B,S-1-4	Land-snail Shells	10.1	19.3	Unit B	4	-7.90	0.31
TEC,B,S-1-7	Land-snail Shells	10.1	19.3	Unit B	7	-7.81	1.49
TEC,B,S-1-10	Land-snail Shells	10.1	19.3	Unit B	10	-7.36	-0.77
TEC,B,S-1-13	Land-snail Shells	10.1	19.3	Unit B	13	-7.69	-0.92
TEC,B,S-1-16	Land-snail Shells	10.1	19.3	Unit B	16	-7.89	0.17
TEC,B,S-1-19	Land-snail Shells	10.1	19.3	Unit B	19	-7.35	-0.29
TEC,B,S-1-22	Land-snail Shells	10.1	19.3	Unit B	22	-7.71	-0.66
TEC,B,S-1-25	Land-snail Shells	10.1	19.3	Unit B	25	-7.90	-0.03
TEC,B,S-2-1	Land-snail Shells	9.0	18.5†	Unit B	1	-9.61	-0.94
TEC,B,S-2-4	Land-snail Shells	9.0	18.5†	Unit B	4	-9.19	-0.98
TEC,B,S-2-7	Land-snail Shells	9.0	18.5†	Unit B	7	-9.46	-1.31
TEC,B,S-2-10	Land-snail Shells	9.0	18.5†	Unit B	10	-9.06	-0.95
TEC,B,S-2-13	Land-snail Shells	9.0	18.5†	Unit B	13	-9.12	-0.93
TEC,B,S-2-16	Land-snail Shells	9.0	18.5†	Unit B	16	-9.52	-1.01
TEC,B,S-2-19	Land-snail Shells	9.0	18.5†	Unit B	19	-9.57	-0.89
TEC,B,S-2-22	Land-snail Shells	9.0	18.5†	Unit B	22	-10.30	-1.06
TEC,B,S-2-25	Land-snail Shells	9.0	18.5†	Unit B	25	-9.61	-1.17
TEC-99,B,S-3-1	Land-snail Shells	9.9	20.9	Unit B	1	-8.94	-1.73
TEC-99,B,S-3-4	Land-snail Shells	9.9	20.9	Unit B	4	-9.20	-0.86
TEC-99,B,S-3-7	Land-snail Shells	9.9	20.9	Unit B	7	-10.53	-0.31
TEC-99,B,S-3-10	Land-snail Shells	9.9	20.9	Unit B	10	-10.47	-0.51
TEC-99,B,S-3-13	Land-snail Shells	9.9	20.9	Unit B	13	-10.31	-0.28

TEC-99,B,S-3-16	Land-snail Shells	9.9	20.9	Unit B	16	-10.34	-0.85
TEC-99,B,S-3-19	Land-snail Shells	9.9	20.9	Unit B	19	-10.26	-1.08
TEC-99,B,S-3-22	Land-snail Shells	9.9	20.9	Unit B	22	-10.50	-0.48
TEC-99,B,S-3-25	Land-snail Shells	9.9	20.9	Unit B	25	-9.99	-1.05

† - measurement may not be accurate due to slight shell damage
n.d. – not determined but similar to other shells analysed
n.a. – not applicable

Table S6. Grand means of stable carbon- and oxygen-isotope data ($\delta^{13}C$, $\delta^{18}O$) from the shells of modern and fossil land snails (*Bothriembryon sayi*) utilized in this study. Unit averages and ranges of $\delta^{13}C$ and $\delta^{18}O$ of land-snail shells from Tight Entrance Cave. Grand means and standard errors (S.E.) were calculated from the average values and isotope ranges of individual shell from each unit.

Unit/Age	**Age range (ka)**	**No. of Shells**	**$\delta^{13}C$ V-PDB¥ (‰)** Grand mean of shell averages	**S.E. (±1σ)**	**$\delta^{18}O$ V-PDB (‰)** Grand mean of shell averages	**S.E. (±1σ)**	**$\delta^{18}O$ V-PDB (‰)** Grand mean of shell averages Ice Volume Correction^	**S.E. (±1σ)**	**$\Delta d^{13}C$ V-PDB (‰)** Grand mean of shell ranges	**S.E. (±1σ)**	**$\Delta d^{18}O$ V-PDB (‰)** Grand mean of shell ranges	**S.E. (±1σ)**
Modern	0	4	-8.9	0.5	-0.6	0.1	-0.6	0.1	1.1	0.2	0.9	0.1
Unit J	33–29	5	-6.9	0.3	0.2	0.2	-0.6	0.2	2.7	0.3	2.0	0.4
Unit H	37–32	3	-7.6	0.3	-0.3	0.3	-1.1	0.3	1.6	0.2	1.4	0.4
Unit F2/F1	53–44	7	-8.7	0.7	-0.5	0.2	-1.1	0.2	1.7	0.2	1.8	0.2
Unit E*	74–66	3	-9.9	1.3	-1.2	0.2	-1.8	0.2	1.6	0.3	1.6	0.3
Unit D	119–89	6	-11.4	0.5	-1.1	0.1	-1.4	0.1	1.2	0.3	1.2	0.2
Unit B	151–135	3	-9.1	0.7	-0.7	0.3	-1.6	0.3	1.1	0.3	1.4	0.6

¥ modern samples corrected by +1.5‰ for the effects of fossil fuel burning over the past 200 years (Friedli *et al.* 1986).

^ Ice volume corrections were made using the ice volume $\delta^{18}O$ estimates of Bintanja *et al.* (2008).

Table S7. $\delta^{13}C$ estimates of modern kangaroo diets in the Tight Entrance Cave region. Tooth enamel $\delta^{13}C$ values were converted into corresponding dietary $\delta^{13}C$ values using an εe-d of 13.3‰ (Prideaux *et al.* 2009).

Sample ID	Year Collected	Latitude (°S)	Longitude (°E)	Species	Sample type/ tooth	$\delta^{13}C$ PDB
2003.1.29-47	2003	34.34	116.38	*Macropus fuliginosus*	stomach contents	-30.0
2003.1.29-68	2003	34.39	116.49	*Macropus fuliginosus*	stomach contents	-28.9
2003.1.29-32	2003	34.83	116.04	*Macropus fuliginosus*	st. contents/faeces	-29.4
2003.1.29-54	2003	34.37	116.39	*Macropus* sp.	faeces	-29.0
2003.1.29-59	2003	34.39	116.49	*Macropus* sp.	faeces	-30.2
2003.1.29-65	2003	34.39	116.49	*Macropus* sp.	faeces	-29.8
2003.1.29-28	2003	34.82	116.06	*Macropus* sp.	faeces	-29.2
2003.1.29-7	2003	34.77	116.08	*Macropus* sp.	faeces	-29.5
2003.1.29-37	2003	34.83	116.04	*Macropus fuliginosus*	stomach contents	-28.9
2003.1.29-37	2003	34.83	116.04	*Macropus fuliginosus*	m4	-27.4
2003.1.29-36	2003	34.83	116.04	*Macropus fuliginosus*	m3	-27.0
2003.1.29-23	2003	34.82	116.06	*Macropus fuliginosus*	m4	-27.3
2003.1.29-11	2003	34.80	116.07	*Macropus fuliginosus*	m4	-26.5
2003.1.29-3	2003	34.73	116.09	*Macropus fuliginosus*	m4	-27.0
2003.1.29-3	2003	34.73	116.09	*Macropus fuliginosus*	m4	-27.9
2003.1.29-12	2003	34.80	116.07	*Macropus fuliginosus*	m3	-27.4
2003.1.29-30	2003	34.82	116.06	*Macropus fuliginosus*	m3	-27.6
WAM M7687*	1967	32.80	116.20	*Macropus irma*	m4	-27.6
WAM M14437*	1975	34.41	116.35	*Macropus irma*	m4	-27.5

* corrected by -0.5‰ according to recent changes in atmospheric CO_2 $\delta^{13}C$ values (Friedli *et al.* 1986).

Interpretation of Land-snail Stable Isotopes

Oxygen Isotopes

This diffusive evaporation model of Balakrishnan and Yapp (2004) currently offers the most comprehensive framework for interpreting land-snail shell $\delta^{18}O$ values in terms of environmental parameters. Fig.S7 outlines the sensitivities of land-snail $\delta^{18}O_{shell}$ to changes in various environmental parameters according to this model.

Figure S7. Modeled land-snail $\delta^{18}O_{shell}$ versus $\delta^{18}O_{rain}$, for given temperature (**A**) and relative humidity (**B**) generated using the diffusive evaporation model of Balakrishnan and Yapp (2004). We assume that ambient water vapor is in isotopic equilibrium with rainwater, and that all of water ingested by the snail is lost via evaporation through the skin (i.e., θ = 0). Vertical and horizontal black bars show the range of modern land-snail $\delta^{18}O_{shell}$ determined for the Tight Entrance Cave site (Table S6) and the range of $\delta^{18}O_{rain}$ measured by Treble *et al.* (2005) for rain collected at the nearby Cape Leeuwin weather station between October 2000 and October 2001.

a b

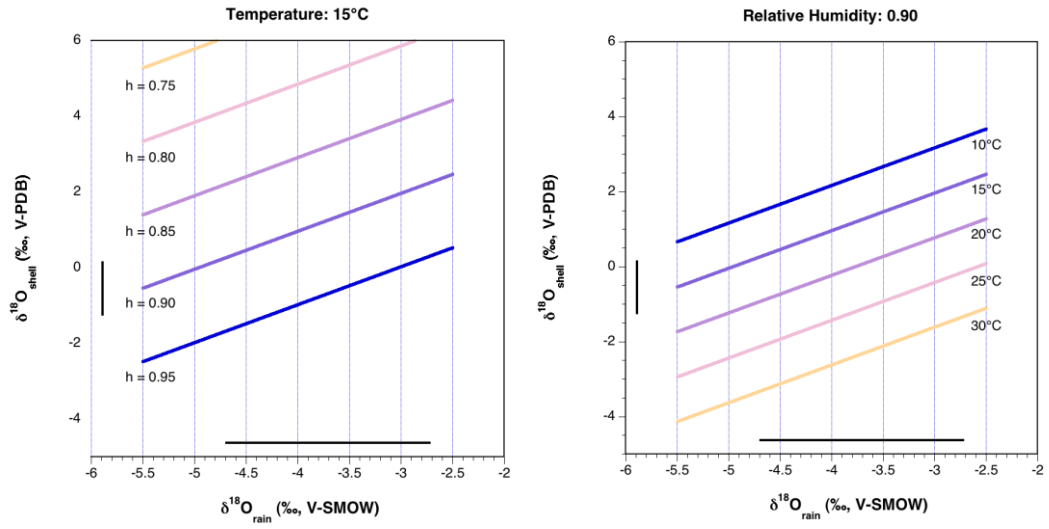

According to the criteria of Balakrishnan & Yapp (2004) climate conditions in the TEC region appear favorable for land-snail activity (and shell growth) throughout most of the year. Present-day temperatures and relative humidities, as recorded at the nearby Bureau of Meteorology weather station at Cape Leeuwin (34.37°S, 115.14°E), range from 11.2°(July) to 23.0°C (January) and 0.81 (9am, July) to 0.76 (9 am, January), respectively (Fig. S8). While the annual rainfall of 971 mm is mainly confined to the winter months, around 53 mm also falls between December to January.

To test how well land-snail shells record environmental parameters at TEC we compared the $\delta^{18}O$ shell from two modern shells with a synthetic isotope time-series generated using the diffusive evaporation model of Balakrishnan & Yapp (2004). Monthly average temperature and relative humidity measurements made at 9 am at the Cape Leeuwin weather station together with the $\delta^{18}O$ estimates for winter (–4.7‰ SMOW, May–October) and summer (–2.3‰ SMOW, November–

Figure S8. (**A**) Monthly averages of relative humidity (green curve) and temperatures (dotted red curve) recorded at 9 am at the Bureau of Meteorology weather station at Cape Leeuwin (http://www.bom.gov.au/climate/averages). Also shown are the seasonal $\delta^{18}O$ amount-weighted means obtained for rain collected at Cape Leeuwin between October 2000 and October 2001 (Treble *et al.* 2005). (**B**) Synthetic land-snail $\delta^{18}O_{shell}$ time-series generated using the diffusive-evaporation of Balakrishnan & Yapp (2004) assuming water vapor in equilibrium with rain and all water ingested by the snail is lost by evaporation (i.e., θ = 0). The model-curves (purple) are calculated with the modern climatology and isotope data shown in (a), and with humidity increased by +0.15 units (dashed purple). Also shown for comparison are the $\delta^{18}O_{shell}$ profiles measured for two modern land snails from the Tight Entrance Cave site (blue and grey). Chronologies for the modern samples have been generated assuming the cyclicity observed in the $\delta^{18}O_{shell}$ values is seasonal.

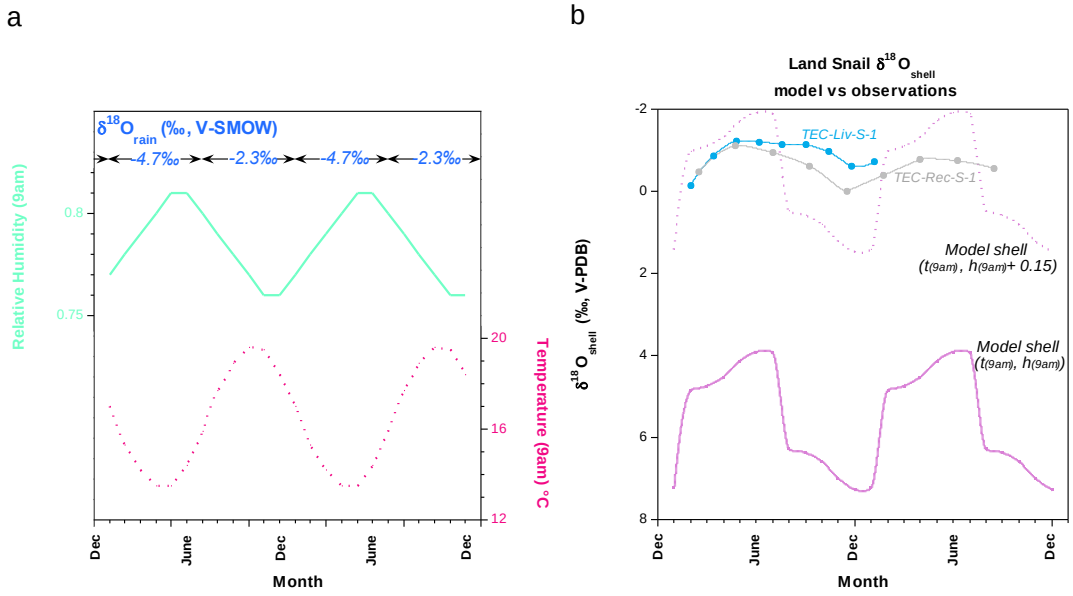

April) rainfall collected at this station (Treble *et al.* 2005) are used as the input parameters in the model calculations (Fig. S8).

The absolute $\delta^{18}O_{shell}$ values predicted by the diffusive evaporation model are offset from those observed for modern land snails (Fig. S8). An offset from model values generated using the 9 am humidity values is perhaps not that surprising as snail activity (and shell formation) will preferentially take place after rainfall events or at night when humidities are likely to be greater than (or equal to) the average values measured at 9 am. Unfortunately we lack the more detailed meteorological data necessary to investigate this further. However it is interesting to note that if relative humidities were between 0.10 and 0.15 humidity units higher than the a priori 9 am measurements during snail shell growth (as would be perhaps be anticipated immediately following rainfall events) much better agreement is seen between model and observational data (Fig. S8).

The range in $\delta^{18}O_{shell}$ values observed for the modern land snail is also markedly attenuated with respect to model predictions (Fig. S8). This discrepancy could result from a bias towards wetter months of the year (when snail activity is likely to be greatest), so some degree of attenuation of the

seasonal $\delta^{18}O_{shell}$ signatures might be anticipated from the analysis of evenly spaced snail shell segments. The other and potentially the primary reason for an attenuated seasonal land-snail $\delta^{18}O_{shell}$ signature most likely stems from the isotopic smoothing accompanying shell formation, and the sampling strategy employed here to generate land-snail $\delta^{18}O_{shell}$ time series (see discussion above).

In summary, the $\delta^{18}O$ results from serially sampled modern land-snail shells from the TEC region are consistent with observational climate data given the nature of shell formation processes, and likely periods of land-snail activity. This suggests $\delta^{18}O$ shell from fossil land snails (sampled using identical sampling protocols) will be a sensitive proxy of past changes in environmental parameters (h, t) and $\delta^{18}O_{rain}$. Specifically, for a fixed $\delta^{18}O_{rain}$ value, increases in fossil land-snail $\delta^{18}O_{shell}$ will be produced by decreases in relative humidities and/or temperatures during the period of shell growth, and vice versa.

Carbon Isotopes

Modern land-snail dietary $\delta^{13}C$ values, calculated using the diffusive evaporation model of Balakrishnan & Yapp (2004), are given in Fig. S9. The model calculations predict that land-snail diets at this site lie entirely within the range of $\delta^{13}C$ values observed for modern C_3 vegetation. The model predictions are in accord with expectation as C_4 grasses are known to be essentially absent in the region from our measurements of the $\delta^{13}C$ of kangaroo (grass) diets (Fig. S9; Table S7), and from direct field observations of C_4 grass abundances (Hattersley 1983). As with the oxygen isotopes of the TEC land snails however, the possibility exists that seasonal biases and/or attenuations arising from two-stage shell calcification are also influencing the $\delta^{13}C_{shell}$ values. Unfortunately we lack the detailed field seasonal vegetation data to put this to the test.

Given that the model of Balakrishnan & Yapp (2004) was able to successfully predict the likely $\delta^{13}C_{diet}$ ($\delta^{13}C_{plant}$) values from our $\delta^{13}C_{shell}$ data, we feel confident in applying it to the fossil land-snails shells at TEC. Fig. S9b shows the results of these model calculations. Land snails from unit J (33–29 ka) yield the highest $\delta^{13}C_{diet}$ estimates while those from Unit D (119 – 89 ka) the lowest, but all lie within range of values of C_3 plants (Fig. S9b, Table S5). This suggests that the food source of land snails at the TEC site has been dominated by C_3 plants for the past 150 kyr.

The equation below outlines the main factors determining $\delta^{13}C$ values ($\delta^{13}C_{C3}$) of C_3 plants (Farquhar *et al.* 1982), viz:

$$\delta^{13}C_{C3} = \delta^{13}C_{CO2} - a - (b - a)\, p_i / p_a$$

where:

a - diffusion of CO_2 into leaf (4.4 ‰)
b - carboxylation of Rubisco (27 ‰)
$p_{i,\,a}$ - pCO_2 inside leaf (i), atmosphere (a)

$\delta^{13}C_{C3}$ is very sensitive to changes in p_i which can change markedly in response to water stress. In summer to conserve water C_3 plants will narrow their stomata thereby reducing p_i/p_a leading to $\delta^{13}C$ enriched in ^{13}C. The $\delta^{13}C$ of land-snail C_3 plant food sources should therefore be sensitive to the water-stresses experienced throughout the year, and it would be expected that the spread of their $\delta^{13}C_{shell}$ values should reflect the extent of this. All other things being equal, it is anticipated that changing from a closed-canopy densely forested setting to one that is more open is likely to result in substantial increases in water stress levels experienced by plants, and corresponding increases in the ranges of land-snail $\delta^{13}C_{shell}$ values. In this connection it is interesting to note that land snails from Unit J have the largest spread in shell $\delta^{13}C$ values (Table S5).

Figure S9. Dietary $\delta^{13}C$ estimates for (**A**) modern land snails (red) and modern kangaroos (purple), and (**B**) modern and fossil land snails from the TEC site. Calculations in (**A**) and (**B**) were performed using the diffusive-evaporation model of Balakrishanan & Yapp (2004) assuming loss of CO_2 expelled in body fluids as HCO_3^- is minimal (i.e. $\theta = 0$) and with T=15°C, pCO_2 = 380 ppm (modern), 250 ppm (Unit D (119–89ka)), and 200ppm (Unit E*–J (74–29ka) and Unit B (151–135ka)) (Leuenberger *et al.* 1992). Modern snail diets in (**B**) were calculated using $\delta^{13}C_{shell}$ values corrected (by +1.5‰) for the effects of fossil fuel burning (Friedli *et al.* (1986)). $\delta^{13}C$ estimates of kangaroo (grass) diets from near-by locations are derived from $\delta^{13}C$ values of tooth enamel or plant samples from the intestinal tract (Table S7).

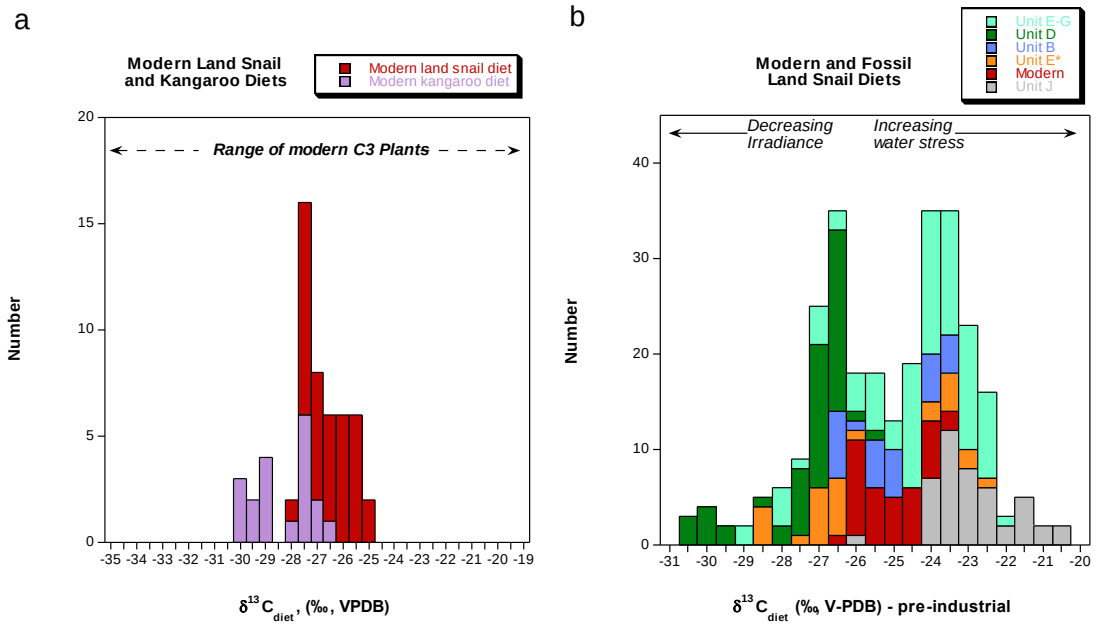

In low light conditions such as those encountered in close-canopy forests, C_3 plants are also commonly found to be highly depleted in ^{13}C (with $\delta^{13}C_{C3}$ = –30 to –35‰, Van der Merwe & Medina 1991). CO_2 recycling from underlying soils depleted in ^{13}C and physiological responses of p_i to irradiance levels (Ehleringer *et al.* 1986; Farquhar *et al.* 1989) likely cause such ^{13}C depletions.

Higher as well as greater ranges in $\delta^{13}C_{shell}$ values from the upper units in the TEC deposit can therefore be regarded as indicating drier conditions/more open canopies.

CHARCOAL RECORD

Methodology

Sediment samples were collected from the southeast wall of the TEC excavation. Successive stratigraphic units are differentiated on the basis of color, mineralogy and stratal geometry (Ayliffe *et al.* 2008; Figs. S10, S11). Sediments consist of moderate to moderately well-sorted coarse sands, poorly to fairly cemented by calcite and authigenic phosphate and interbedded with calcite flowstone. Sands become poorly consolidated up-section, probably reflecting reduced burial compaction and cementation. Samples were collected in continuous 5 cm increments and each sample was spiked with a *Lycopodium* tablet (n=12542, batch 124961), carbonates removed with 5% HCl and silicates removed with a HF acid treatment. Samples were deflocculated with hot 10% NaOH, treated with 4 minutes acetolysis to remove organics and then washed through 200 and 5 μm screens. Macrocharcoal (>200μm) grain diameter and frequency were determined under a low power optical microscope using a grid-square technique and the square of geometric mean diameter used to estimate macrocharcoal concentration (Clark & Hussey 1996). Using a minimum grain count of 200, which estimates concentration to within 5% of a 1000-grain count (Finsinger and Tinner, 2005), point counts of euckette slide preparations were used to estimate microcharcoal (5-200μm) concentration (Clark 1982).

Relationship between charcoal size-classes

Previous studies have indicated that variation in the abundance of charcoal within sedimentary deposits can record fire events at different provenance scales (Clark 1988; Clark *et al.* 1998; Whitlock& Millspaugh 1996; Carcaillet *et al.* 2001; Lynch *et al.* 2004; Ohlson & Tryterud 2000). If macrocharcoal and microcharcoal did have the same source areas they should be strongly correlated. As is indicated by the weak regression between macrocharcoal and microcharcoal, this appears not to be the case at TEC (Fig. S11). The relationship is statistically significant (DF=1, F=9.700, P=0.004) but the coefficient of correlation (R^2) has a value of just 0.244, indicating that less than 25% of variation is shared between the two size fractions. A suite of transformations failed to improve the correlation or its statistical significance. A more comprehensive analysis by Carcaillet *et al.* (2001) using a slightly different mesh size (150μm) and with the addition of comparative analysis of charcoal time-series indicators, obtained a similar result as that reported here (statistical significance but a weak coefficient of correlation), and it was subsequently concluded that some dissociation between scales of charcoal provenance existed. We agree with this view, which suggests that macrocharcoal by virtue of its larger size, reflects primarily locally sourced charcoal. Microcharcoal on the other hand can be transported regionally, following initial

convection in smoke plumes (Clark 1988), and whilst this proxy undoubtedly receives some contribution from local charcoal reservoirs, it reflects a more regional-scale burning pattern.

Charcoal variation with depth

Variation in quantified abundance of macrocharcoal with depth is consistent with visual observations of distinctive charcoal layers at 260–270 cm, 225 cm, 190–200 cm and 180 cm (Fig. S10). Microcharcoal concentrations are orders of magnitude higher than macrocharcoal concentrations, probably reflecting the consistent skew in charcoal production distributions towards smaller particles (Clark *et al.* 1998) as well as methodological variations (such as field of view differences) unique to the respective techniques used to quantify the two size fractions (Clark & Hussey 1996). Clear differences exist in the abundance of large and small charcoal particles in the deposit. A baseline macrocharcoal concentration of ~0.005 mm^2/mL exists throughout the deposit but is punctuated by peaks in abundance almost five times this baseline value. Microcharcoal concentrations exhibit a comparable spread in minimum and maximum values, although above 270 cm there is a clear increasing trend in both minimum and maximum concentrations (Fig. 2B).

For purposes of interpretation, the deposit can separated into three distinct zones bounded by pauses in sedimentation evidenced by flowstone formation. Zone 1 is composed of units B and D (151–89 ka), zone 2 of units E*, F1 and F2 (70–45 ka) and zone 3 of units H and J (35–29 ka). Zone 1 characteristically exhibits lower charcoal concentrations than younger sediments in zones 2 and 3. Highest values in zone 1 occur between 320–350 cm, corresponding to deposition between about 152–90 ka. Overlying charcoal concentrations between 320–270 cm are lower with little variability, but concentrations increase significantly in middle Unit E*, marking a dramatic change in the pattern of charcoal accumulation, especially with respect to the microcharcoal record. The abrupt nature of this change (dated to about 70ka) suggests it is not a taphonomic pattern, especially given it is neither gradual nor clearly associated with a unit boundary (Fig. 2B). Subsequent to this, there is a clear increasing trend in baseline levels of microcharcoal from middle Unit E* (~270 cm) upwards, which correlate with a ^{13}C isotopic enrichment trend over the same interval, supporting its relationship to an increasingly more open environment regionally. Patterns of macrocharcoal concentrations through zones 2 and 3 are perhaps slightly increased, but not markedly dissimilar from those in zone 1. There is apparently little correlation with stable isotopic records from land snail shells, which supports the inference that macrocharcoal in the deposit primarily represents local bush fire events, tied perhaps only loosely to changes in regional climate, and more strongly indicative of local environmental variables such as topography and vegetation (Ohlson & Tryterud 2000; Lynch *et al.* 2007).

Figure S10. Interpreted stratigraphy of the southeast wall. Black arrows identify major visible increases in charcoal content in the deposit. Blue boxes represent the position of the unit with respect to the established datum while transparent bars represent the sampled section for micro- and macrocharcoal analysis.

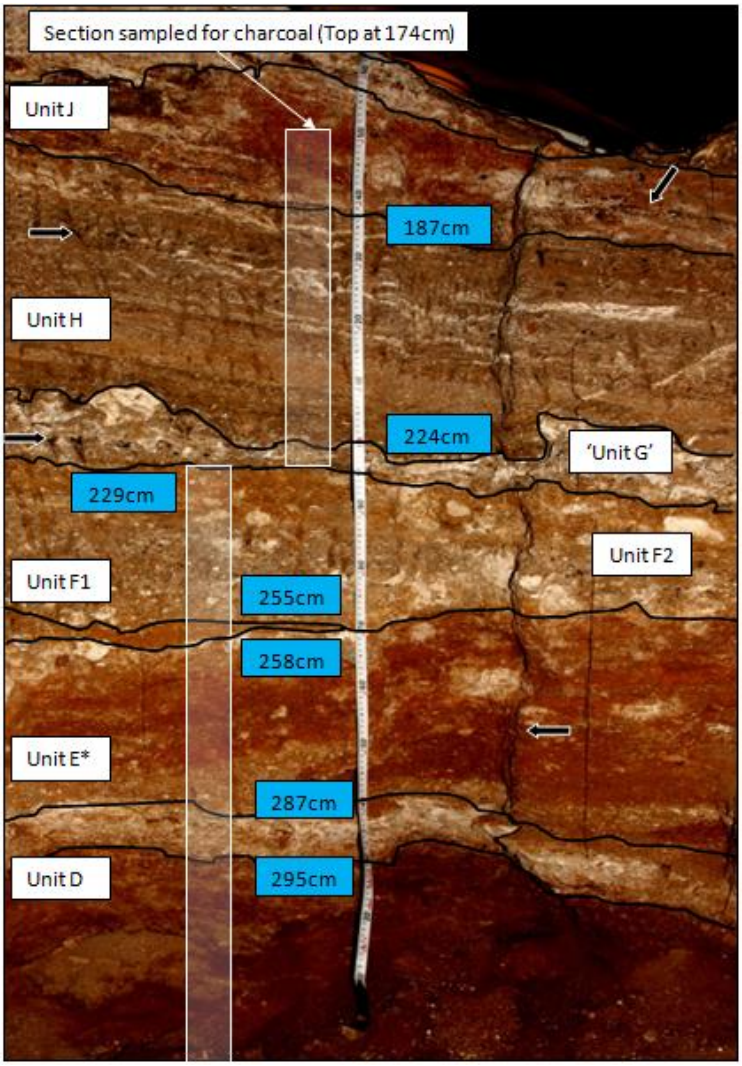

Figure S11. Untransformed linear regression of macrocharcoal against microcharcoal concentrations. Regression analysis demonstrates that there is a significant correlation at α level of 0.05 (DF=1, F=9.700, P=0.004) but a weak coefficient of correlation.

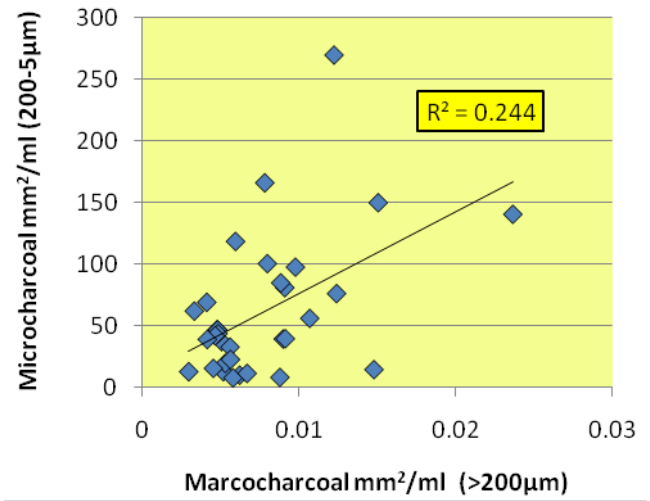

REFERENCES

Aitken MJ (1998) *An Introduction to Optical Dating: the Dating of Quaternary Sediments by the Use of Photon–stimulated Luminescence* (Oxford University Press, New York).

Ayliffe LK *et al.* (2008) Age constraints on Pleistocene megafauna at Tight Entrance Cave in Southwestern Australia. *Quat. Sci. Rev.* 27:1784–1788.

Balakrishnan M, Yapp CJ (2004) Flux balance model for the oxygen and carbon isotope composition of land snail shells. *Geochim. Cosmochim. Acta* 68:2007–2024.

Balakrishnan M *et al.* (2005) Environmental significance of $^{13}C/^{12}C$ and $^{18}O/^{16}O$ ratios of modern land-snail shells from the southern Great Plains of North America. *Quat. Res.* 63:15–30.

Barnosky AD *et al.* (2004) Exceptional record of mid-Pleistocene vertebrates helps differentiate climatic from anthropogenic ecosystem perturbations: *Proc. Nat. Acad. Sci. USA* 101:9297–9302.

Barnosky AD, Carrasco MA, Davis EB (2004) The impact of the species–area relationship on estimates of paleodiversity. *PLoS Biol.* 3:e266.

Bintanja R, van de Wal RSW (2008) North American ice-sheet dynamics and the onset of 100,000-year glacial cycles. *Nature* 454:869–872.

Bøtter–Jensen L, Bulur E, Duller GAT, Murray AS (2000) Advances in luminescence instrument systems. *Radiat. Meas.* 32:523–528.

Bowler JM *et al*. (2003) New ages for human occupation and climatic change at Lake Mungo, Australia. *Nature* 421:837–840.

Carcaillet C *et al.* (2001) Comparison of pollen-slide and sieving methods in lacustrine charcoal analyses for local and regional fire history. *Holocene* 11:467–476.

Cheng H *et al*. (2000) The half-lives of uranium-234 and thorium-230. *Chem. Geol.* 169:17-33.

Clark JS (1988) Particle motion and the theory of charcoal analysis: source area, transport, deposition and sampling. *Quat. Res.* 30:67-80.

Clark JS, Hussey TC (1996) Estimating the mass flux of charcoal from sediment records: the effect of particle size, morphology, and orientation. *Holocene* 8:129-144.

Clark JS, Lynch J, Stocks BJ, Goldammer JG (1998) Relationships between charcoal and particles in air and sediments in west-central Siberia. *Holocene* 8:19-29.

Couzens AM (2007) *Late Pleistocene environmental history from southwestern Australia: No evidence for climate-driven megafauna extinction* (B.Sc.(Hons) Thesis, University of Western Australia, Perth).

Cowie RH (1984) The life-cycle and productivity of the land snail *Theba pisana* (Mollusca: Helicidae). *J. Anim. Ecol.* 53:311–325.

Ehleringer JR, Field CB, Lin ZF, Kuo CY (1986) Leaf carbon isotope ratio and mineral composition in subtropical plants along an irradiance cline. *Oecologia* 70:520-526.

Farquhar GD, Ehleringer JR, Hubick KT (1989) Carbon isotope discrimination and photosynthesis. *Ann. Rev. Plant Physiol. Mol. Biol.* 40:503–537.

Farquhar GD, O'Leary MH, Berry JA (1982) On the relationship between carbon isotope discrimination and the intercellular carbon dioxide concentration in leaves. *Aust. J. Plant. Physiol.* 9:121–137.

Finsinger W, Tinner W (2005) Minimum count sums for charcoal-concentration estimates in pollen slides: reliability and potential errors. *Holocene* 15:293–297.

Francey RJ (1983) A comment on $^{13}C/^{12}C$ in land snail shells. *Earth Planet. Sci. Lett.* 63:142–143.

Friedli H *et al*. (1986) Ice core record of the $^{13}C/^{12}C$ ratio of atmospheric CO_2 in the past two centuries. *Nature* 324:237–238.

Galbraith RF *et al*. (1999) Optical dating of single and multiple grains of quartz from Jinmium Rock Shelter, northern Australia: Part I, experimental design and statistical models. *Archaeometry* 41:339–364.

Goodfriend GA, Hood DG (1983) Carbon isotope analysis of land snail shells: implications for carbon sources and radiocarbon dating. *Radiocarbon* 25:810–830.

Goodfriend GA, Magaaritz M, Gat JR (1989) Stable isotope composition of land snail body water and its relation to environmental waters and shell carbonate. *Geochim. Cosmochim. Acta* 53:3215–3221.

Gully GA (1997) Tight Entrance Cave, south-western Australia: a new megafaunal site and its palaeoclimatic and biogeographic implications (B.Sc. (Hons) Thesis, Flinders University, Adelaide).

Hattersley PW (1983) The distribution of C3 and C4 grasses in Australia in relation to climate. *Oecologia* 57:113–128.

Helgen KM *et al.* (2006) Ecological and evolutionary significance of sizes of giant extinct kangaroos. *Aust. J. Zool.* 54:293–303.

Hellstrom JC (2003) Rapid and accurate U/Th dating using parallel ion-counting multicollector ICP-MS. *J. Anal. At. Spectrom.* 18:1346-1351.

Hellstrom JC (2006) U–Th dating of speleothems with high initial 230Th using stratigraphical constraint. *Quat. Geochron.* 1:289–295.

Huntley DJ, Godfrey-Smith DI, Thewalt MLW (1985) Optical dating of sediments. *Nature* 313:105–107.

Jacobs Z, Duller GAT, Wintle AG (2006) Interpretations of single grain De distributions and calculation of De. *Radiat. Meas.* 41:264–277.

Jacobs Z, Roberts RG (2007) Advances in optically stimulated luminescence dating of individual grains of quartz from archaeological deposits. *Evol. Anthrop.* 16:210–223.

Jacobs Z *et al.* (2008) Equivalent dose distributions from single grains of quartz at Sibudu, South Africa: context, causes and consequences for optical dating of archaeological deposits. *J. Archaeo. Sci.* 35:1808–1820.

Johnson, CN, Prideaux GJ (2004) Extinctions of herbivorous mammals in Australia's late Pleistocene in relation to their feeding ecology: no evidence for environmental change as cause of extinction. *Aust. Ecol.* 29:553–557.

Leuenberger M, Siegenthaler U, Langway C (1992) Carbon isotope composition of atmospheric CO_2 during the last ice age from an Antarctic ice core. *Nature* 357:488–490.

Lynch AH *et al*. (2007) Using the paleorecord to evaluate climate and fire interactions in Australia. *Ann. Rev. Earth Planet. Sci.* 35:215–239.

Lynch JA, Clark JS, Stocks BJ (2004) Charcoal production, dispersal and deposition from the Fort Providence experimental fire: interpreting fire regimes from charcoal records in boreal forests. *Can. J. Forest Res.* 34:16-42.

Margaritz M, Heller J, Volokita M (1981) Land-air boundary environment as recorded by the $^{18}O/^{16}O$ and $^{13}C/^{12}C$ isotope ratios in the shells of land snails. *Earth Planet. Sci. Lett.* 52:101–106.

Murray AS, Roberts RG (1998) Measurement of the equivalent dose in quartz using a regenerative–dose single–aliquot protocol. *Radiat. Meas.* 29:503–515.

Murray AS, Wintle AG (2000) Luminescence dating of quartz using improved single–aliquot regenerative–dose protocol. *Radiat. Meas.* 32:57–73.

Ohlson M, Tryterud E (2000) Interpretation of the charcoal record in forest soils: forest fires and their production and deposition of macroscopic charcoal. *Holocene* 10:519–525.

Prescott JR, Hutton JT (1994) Cosmic ray contributions to dose rates for luminescence and ESR dating: large depths and long–term time variations. *Radiat. Meas.* 23:497–500.

Prideaux GJ (1999) *Borungaboodie hatcheri* gen. et sp. nov., a very large bettong (Marsupialia: Macropodoidea) from the Pleistocene of southwestern Australia. *Rec. W. Aust. Mus.* Supp. 57:317–329.

Prideaux GJ *et al*. (2009) Extinction implications of a chenopod browse diet for a giant Pleistocene kangaroo. *Proc. Nat. Acad. Sci. USA* 106:11646-11650.

Raup DM (1975) Taxonomic diversity estimation using rarefaction. *Paleobiol*. 1:333–342.

Roberts RG *et al.* (2000) Distinguishing dose populations in sediment mixtures: a test of single–grain optical dating procedures using mixtures of laboratory–dosed quartz. *Radiat. Meas.* 32:459–465.

Roberts RG *et al.* (2001) New ages for the last Australian megafauna: continent-wide extinction about 46,000 years ago. *Science* 292:1888–1892.

Treble PC *et al.* (2005) In situ measurement of seasonal $\delta^{18}O$ variations and analysis of isotopic trends in a modern speleothem from southwest Australia. *Earth Planet. Sci. Lett.* 233:17–32.

van der Merwe NJ, Medina E (1991) The canopy effect, carbon isotope ratios and foodwebs in Amazonia. *J. Archaeo. Sci.* 18:249–259.

van Dyck S, Strahan R (2008) *Mammals of Australia, 3rd ed.* (Reed New Holland, Sydney).

Whitlock C, Millspaugh SH (1996) Testing the assumptions of fire history studies: an examination of modern charcoal accumulation in Yellowstone National Park, USA. *Holocene* 6:7-15.

Wroe S, Argot C, Dickman CR (2004) On the rarity of big fierce carnivores and primacy of isolation and area: tracking large mammalian carnivore diversity on two isolated continents. *Proc. R. Soc. Lond. B* 271:1203–1211.

Yapp CJ (1979) Oxygen and carbon isotope measurements of land snail shell carbonate. *Geochim. Cosmochim. Acta* 43:629–635.